Siliciclastic sediment volumes and rates of the North Pyrenean Retro-Foreland Basin

Alexandre Ortiz, François Guillocheau, Cécile Robin, Eric Lasseur, Justine Briais, Charlotte Fillon

SILICICLASTIC SEDIMENT VOLUMES AND RATES OF THE NORTH PYRENEAN RETRO-FORELAND BASIN

Alexandre Ortiz[1], François Guillocheau[1], Cécile Robin[1], Eric Lasseur[2], Justine Briais[2], Charlotte Fillon[3]

1: Univ Rennes, CNRS, Géosciences Rennes - UMR 6118, 35000 Rennes, France

2: BRGM (French Geological Survey), 45060 Orléans Cedex 2, France

3: TotalEnergies, Research and Development, 64018 Pau Cedex, France

Corresponding author[1]: Alexandre ORTIZ

Univ Rennes, CNRS, Géosciences Rennes - UMR 6118, 35000 Rennes, France

Email address: alex.ortiz@hotmail.fr

[1] Present-day affiliation : BRGM (French Geological Survey), 45060 Orléans Cedex 2, France

Acknowledgments

This work is part (and supported by) the 'Source-to-Sink compression' project that is jointly managed by TotalEnergies and the French geological survey BRGM. The original manuscript was significantly improved by the editor, Cari Johnson and the contribution of John M Holbrook and anonymous reviewer during the peer-review process.

Abstract

Sediment accumulation rates in foreland basins results from a complex interplay between surface and deep processes in both the exhumed relief domain and sedimentary basins. The growth and decay of a mountain belt during orogenic and post-orogenic phases have been largely studied thanks to thermochronological and structural studies. The sedimentary response of the orogenic phases in the preserved sediments of the surrounding basins is well known in terms of sedimentary filling patterns and architecture, but much less better quantified.

Here, we performed a measurement of the siliciclastic sediment volumes of the Pyrenean retro-foreland basin – the Aquitaine Basin and the Bay of Biscay during Cenozoic times – for a better understanding of the erosion and the sediment transfer and deposition during the convergence (syn-orogenic) to post-convergence (post-orogenic) periods of the Pyrenees Mountain. The measurement of the compacted siliciclastic sediment is based on sediment

thickness (isopach) maps of known lithologies, derived from the interpretation of 40 000 kms of seismic profiles.

Thanks to the siliciclastic sediment volumes quantification and a well-known retro-foreland basin tectono-sedimentary evolution, we bring quantitative results as:

(1) The amount of preserved sediments is of 51 500 ± 16 800 km^3 for the Cenozoic.

(2) The siliciclastic sediment rate curve during Cenozoic shows two major increase around 26.0 Ma and 2.5 Ma. The 26.0 Ma increase is clearly related to the erosion of the Pyrenees of tectonic origin. The major 2.5 Ma one would be mainly related to a climatic forcing.

(3) The mass balance between the Aquitaine Platform and the deepest domains change through time in favour of the deep domain. This might be explained by the ratio between subsidence that created accommodation space and the sediments feed by the mountain belt and stored in the Aquitaine Platform.

Keywords: accumulation rates, retro-foreland, Pyrenees, Aquitaine Basin, Bay of Biscay, Cenozoic

1. Introduction

The growth and decay of mountain belts reliefs result from feedbacks between convergence rates, surface processes (Beaumont et al., 1992; Willett, 1999) and isostatic response (Molnar and Lyon-Caen, 1988; Watts, 2001). The topography of a mountain belt is first built by continental crust thickening during convergence, generating loading on the lithosphere and its downward deflection at the origin of the surrounding foreland basins and their vertical motion (Beaumont, 1981; Allen and Allen, 2013). Topographic evolution of the mountain belt is also influenced by climate which can modify the erosion by surface processes (e.g. Whipple, 1999). Finally, the base level variations in the foreland basins may play a dominant role, on piedmont dynamics, in preserving reliefs (base level rise with emplacement of endorheism, Babault et al., 2005) or enhancing its incision (base level fall by major capture for instance, see Burbank and Anderson, 2009)

The estimation of denudation, i.e. the amount of eroded rocks, through time and its controls by lithospheric deformation and/or climate (precipitation) are of primary importance for understanding (1) the topographic growth and decay of mountain belts, but also (2) the volumes and lithologies of the sediments produced and transferred to the surrounding basins. The quantification of the denudation of a mountain belt is mainly based on low temperature chronology (e.g. fission track and (U-Th)/He on apatite and zircons – ZFT, AFT, ZHe, AHe) that

94 provides a cooling history classically converted into exhumation with using thermal numerical
95 models (Braun, 2003 for instance, Ketcham, 2005; Gallagher et al., 2009). The sediment
96 production (volumes, petrography and grain-size) was performed on several foreland basins
97 (Molnar and England, 1990; Einsele, 2000; Najman and Garzanti, 2000; Goodbred and Kuelh,
98 2000; Schlunegger et al., 2001; Garzanti, 2019). In the Pyrenean domain, the P. Allens's group
99 has carried out numerous studies on these thematic, focus on the southern side (e.g. Michael
100 et al., 2013, 2014 a,b; Armitage et al., 2015).
101 The quantification of the siliciclastic sediment volume (sink) in foreland basins was first
102 performed at mountain-scale in the Alps (England, 1981, Kuhlemann, 2000; Kuhlemann et al.,
103 2002), but most of them concerns the latest deposition stages found in the ultimate sink: the
104 passive margin laterally connected to the foreland basins. This is the case for Asian mountains
105 (Métivier et al., 1999; Clift et al., 2006) or Rocky Mountains and the margins of the Gulf of
106 Mexico (Galloway and Williams, 1991; Galloway et al., 2011). They all show an increase of the
107 sedimentation rates up to today, a critical point discussed by P. Molnar (Molnar and England,
108 1990; Molnar, 2004) that might be related to global climate cooling (e.g. Herman and
109 Champagnac, 2016) and/or large erosion/recycling of the foreland deposits (Schlunnegger and
110 Mosar, 2011; Leroux et al., 2017), linked frontal accretion, climate variations and drainage
111 network reorganization. Thus, the volumes distribution (storage, transfer, recycling) between
112 the foreland and the final sink at different stages of mountain belt evolution have not been
113 fully explored since the synthesis of Hinderer, 2012.
114
115 We propose in this study to measure the siliciclastic sediment volumes in a retro-
116 foreland basin where limited frontal accretion allows a more complete preservation of syn-
117 tectonic deposits – the Aquitaine Basin and the Bay of Biscay during Cenozoic times for a

118 better understanding of the erosion, the sediment transfer and deposition during the
119 convergence to post-convergence periods of the Pyrenees Mountains and discuss at the first
120 order the tectonic and climatic control factors. The measurement of the compacted siliciclastic
121 sediment volumes (for a solid rocks equivalence) are based on sediment thickness (isopach)
122 maps of known lithologies, built from an extensive dataset of seismic lines interpreted using
123 the principles of seismic stratigraphy and dated on wells (Ortiz et al., 2020).
124
125 **2. Geological setting**
126
127 The North Pyrenean retro-foreland and its lateral deep area of ultimate sediment
128 deposition – the deep Bay of Biscay Basin – is segmented into three geographical-geological
129 units (Fig. 1): (1) upstream, bounded westward by the Pamplona transfer zone, the Aquitaine
130 Platform (i.e. the modern onshore Aquitaine Basin and its shelf), (2) the Landes Plateau,
131 bounded westward by the Santander "soft" transfer zone, is a step (1000-1800 m deep)
132 bounded by slopes and canyons (Capbreton, Cap-Ferret) and (3) the deep Bay of Biscay (4000-
133 4500 m deep).
134
135 **2.1. Tectonic, relief and exhumation evolution of the Pyrenees**
136
137 The Pyrenees Mountains are a collisional belt bringing Eurasian lithosphere over the
138 Iberian lithosphere (e.g. Roure et al., 1989; Muñoz, 1992). Both Pyrenees and Basque-
139 Cantabrian Mountains result from the inversion and compression of the Albian hyperextended
140 Eurasian lithosphere (e.g. Fabriès et al., 1991, 1998; Lagabrielle et Bodinier, 2008; Jammes et
141 al., 2009; Lagabrielle et al., 2010; Masini et al., 2014; Clerc et al., 2012, 2016; Ducoux et al.,

2019; Saspiturry et al., 2019; Ducoux et al., 2021, Tugend et al., 2014). The relative motion of Eurasia and Africa plates controlled the orogeny: the compression started at the time of convergence of the two plates, i.e. at the end of the Santonian (83.6 Ma, Schettino and Turco, 2011) and ended around the Oligocene-Miocene boundary (chron 6c, Roest and Srivastava, 1991, Macchiavelli et al., 2017).

Thermochronological data also document the early mountain building with a cooling phase at around 70 Ma (Whitchurch et al., 2011; Beamud et al., 2011; Mouthereau et al., 2014; Ternois et al., 2019; Waldner et al., 2021). During Cenozoic, several studies resolve the increase of exhumation during late Eocene-Oligocene times (Fitzgerald et al., 1999; Sinclair et al., 2005; Gibson et al., 2007; Jolivet et al., 2007; Gunnel et al., 2009; Metcalf et al., 2009; Whitchurch et al., 2011; Fillon and van der Beek, 2012; Bosch et al., 2016) following an earlier uplift of the eastern range during Middle Eocene times (Maurel et al., 2008; Beamud et al., 2011; Mouthereau et al., 2014; Vacherat et al., 2014; 2016; Ternois et al., 2019; Whitchurch et al., 2011; Waldner et al., 2021). Finally, a late Miocene exhumation phase is recorded in the Western Pyrenean Range by several authors (Jolivet et al., 2007; Bosch et al., 2016; Fillon et al., 2021)

2.2. Stratigraphic and tectonic evolution of the Aquitaine Basin and Bay of Biscay deep Basin

Several studies have been carried out on the tectono-stratigraphic evolution of the Aquitaine Basin since the late Cretaceous (Brunet, 1984; Desegaulx and Brunet, 1990; Brunet, 1994; Sztrákos et al., 1998; Serrano et al., 2001; Ford et al., 2016; Sztrákos and Steurbaut, 2017; Angrand et al., 2018). They identified two subsiding phases (Latest Santonian - Danian and Thanetian – Oligocene) separated by the so called “Palaeocene quiet period” characterized by a low to near zero subsidence phase (Ford et al., 2016). The first subsidence

166 phase has been largely influenced by the post rift thermal subsidence because of the short
167 time between the end of the rifting and the beginning of the convergence (around 10 Ma,
168 Angrand et al., 2018). Serrano et al., (2001) differentiate two distinct phases in the Western
169 Aquitaine Basin (1) from Palaeocene to Middle Eocene - compressional basin due to
170 lithospheric buckling (mixed system – East-West oriented turbidites and carbonates platform)
171 and (2) from Middle Eocene to Oligocene – foreland stage (progressive continentalization on
172 the eastern part and deltaic progradation toward the West).

173 Recently, through an extensive bio- and seismic stratigraphy study of both basins, Ortiz
174 et al. (2020) identified a set of several discontinuities of tectonic origins (fig. 2). The orogenic
175 period is subdivided into two steps (fig. 2): (1) the dominant lithosphere flexure with the
176 formation of foredeeps up to the uppermost Lutetian and (2) the propagation of the
177 deformation from the orogenic wedge through the basin mainly along salt-controlled thrusts
178 and anticlines locating subbasins. From the basin record point of view, the transition between
179 orogenic and post-orogenic periods is Chattian in age, from 27.1 to 25.2 Ma. This time interval
180 corresponds to the end of thrusting/inversions and a modification of the sediment
181 preservation pattern. The post-orogenic period is also subdivided into two intervals (fig. 2):
182 (1) a sharp decrease of the subsidence rates over the Aquitaine Platform, mainly filled by
183 continental sediments during early Miocene times (25.2-16.4 Ma) and (2) an uplift of the
184 Aquitaine Platform from 16.4 Ma to today characterized by a low-preservation domain up to
185 10.6 Ma. The main uplift phase occurred at 10.6 Ma and caused a generalized by-pass on the
186 Aquitaine Platform (Ortiz et al., 2020).

187

188 **3. Measurement of siliciclastic sediment volumes and rates**

189

The measurement of siliciclastic sediment (sink) volumes is based on four sediment thickness (isopach of preserved sediments) maps: Palaeocene-Eocene (66-33.9 Ma - fig. 3), Oligocene (33.9-23.03 Ma - fig. 4), Miocene (23.03-5.3 Ma - fig. 5) and Pliocene-Pleistocene (5.3-0 Ma - fig. 6). These isopach maps are the products of a seismic stratigraphic analysis of an extensive seismic line dataset (TotalEnergies, BRGM, BSS, fig. 1). This quite low time-resolution is due to the absence of wells in the deep Bay of Biscay and the difficulty to extend timelines from the Aquitaine Platform where several dated wells are available (see Ortiz et al., 2020). For each interval the main lithologies proportion is known in the Aquitaine platform and in the Landes Plateau (see Ortiz et al., 2020) and for the distal part of the Bay of Biscay, we used the studies available in this domain about the Cenozoic sedimentary record (Cremer, 1983; Iglesias, 2009; Brocheray et al., 2014).

The sediment volumes measured from the isopach maps were later decompacted and the amount of sediments produced in the basin (here mainly carbonates) was removed to get solid rock volumes. We used the protocol and code published by Guillocheau et al. (2012) that consider uncertainties or ranges for (1) time-depth conversion parameters, (2) absolute ages of the different horizons, (3) carbonate content and (4) surface porosity and e-folding depth for porosity decrease. During Cenozoic times the deep-sea Bay of Biscay fan fed through the Capbreton and Cap-Ferret Canyon by the sediments coming from the Aquitaine Basin has progressively migrated westward (Cremer, 1983; Iglesias, 2009; Brocheray et al., 2014), our calculation area is evolving accordingly (dashed line on figs, 3, 4, 5, 6). In order to compare the volumes, they will be presented through the evolution of the ratio between Aquitaine Basin volume (V_{On}) and Bay of Biscay volume (V_{Off}) as follow: $R_{OnOff} = V_{On}/V_{Off}$.

4. Isopach maps: results and interpretation

4.1. Paleocene-Eocene (66-33.9 Ma)

The *Paleocene-Eocene* (66-33.9 Ma - Fig. 3) time interval is characterized by sediment preservation along the North Pyrenean Thrust on the Aquitaine Platform, with three subsiding domains - 10-50 km large - filled by 3500 m of sediments accumulated in 32 Ma. Two less subsiding domains were located north of the previous ones and bounded by two ridges with very low accumulation. Few sediments were preserved along the Landes Plateau. In the deep Bay of Biscay, two depocenters occurred south of the South Armorican Margin and north of the Biscay Wedge Front.

Interpretation: The three subsiding domains correspond to a segmented foredeep (Ortiz et al., 2020) controlled by the inherited structures from the Early Cretaceous rifts history (Angrand et al., 2018). These domains are mainly filled during the first orogenic phase (up to uppermost Lutetian) and the small depocenter in the northern part of the ridges correspond mainly to the second orogenic phase, when the deformation is propagated basinward. The two deep depocenters of the Bay of Biscay are disconnected from the Aquitaine Platform and bounded by the inverted extensional structures of the Gascogne Dome Bulge (Thinon, 1999; Thinon et al., 2001). The first depocenter located in the Armorican subbasin, was fed by sediments coming from the Loire River (fig. 1) or from the Armorican Massif (Guillocheau et al., 2003).

4.2. Oligocene (33.9-23.03 Ma)

The *Oligocene* (33.9-23.03 Ma - fig. 4) was a period of more widely distributed sediments accumulation along the three domains. In the Aquitaine Platform depocenters are located (i) on both sides of salt-related controlled thrusts forming anticlines or ridges (Maubourguet-Antin, Audignon) or (ii) along N140° faults (e.g. Téthieu Fault, location on figures 1 and 4). In the south Landes Plateau, north of the Basque-Cantabrian Mountains, a 60 km-large depocenters occurred. In the deep Bay of Biscay, a NW-SE trending depocenter is located south-west of the inverted structures of the Gascogne Dome Bulge and north of the Biscay Wedge Front.

Interpretation: Oligocene is a period during which (1) segmented foredeep was no longer subsident and (2) compressive deformation propagated from the orogenic wedge to the retro-foreland basin along salt decollement levels localizing little subbasins (Serrano, 2001; Ortiz et al., 2020). The depocenters of the south Landes Plateau may be due to the loading effect of the inverted and thrusted Basque Cantabrian Margin starting at 37 Ma and ending at 28.5 Ma (Gomez et al., 2002). The depocenter of the deep Bay of Biscay is disconnected from the Aquitaine Platform and moderately fed by the erosional product coming from the inversion and deformation of the Cantabrian Margin and the uplift of the Cantabrian Mountains from Late Eocene to Oligocene times (Gallastegui et al., 2002; Pedreira et al., 2015; Fillon et al., 2016).

4.3. Miocene (23.03-5.3 Ma)

The *Miocene* (23.03 to 5.3 Ma – fig. 5) recorded a major change in the sediment distribution. The Aquitaine platform was henceforth a place of low sediment preservation (less than 200 m for 17.5 Ma). Most of the sediments were transferred and stored along the

Landes Plateau and the deep Bay of Biscay. Two major sediment accumulations were active in the Landes Plateau, (1) to the north, a progradational wedge (Ortiz et al., 2020) located at the transition between the southeastern part of the South Armorican shelf and the Landes High and (2) to the south, an E-W trending depocenter located north of the Capbreton canyon. The preserved sediments along the deep Bay of Biscay are organized as an E-W trending body more than 100 km-large located on the Biscay Wedge Front. It is upstream in connection with the two depocenters of the Landes Plateau.

Interpretation: The Aquitaine Platform was no longer a significant subsiding domain. Most of the sediments bypassed to deepest areas: (1) through deltaic progradational wedges on the Landes Plateau, (2) through canyons and at the end of the system (3) as deep-sea fans. The depocenters located north to the Capbreton canyon correspond to the northern levee of the canyon already active at this period (Cremer, 1983; Iglesias, 2009, Ortiz et al., 2020). Progradationnal deltaic wedge accumulate at the head of the Cap-Ferret canyon (western extension of the north Landes Plateau depocenter – Cremer, 1983) and downstream (East of the deep Bay of Biscay depocenter), an erosion domain where the canyon is active. These two canyons domains fed downward, the Cap-Ferret deep-sea fan (Cremer, 1983; Iglesias, 2009) in the deep Bay of Biscay.

4.4. Plio-Pleistocene (5.3-0 Ma)

The *Pliocene-Pleistocene* (5.3-0 Ma – fig. 6) time-interval shows an accentuation of the sediment distribution pattern established during Miocene. (1) No to very few sediments were preserved on the Aquitaine Platform. (2) Two depocenters occurred on the Landes Plateau: (i) a N-S trending one north to the Landes High (progradationnal wedges – Ortiz et al., 2020) and

285 (ii) a N-S trending one south of the Landes High. (3) The depocenters of the deep Bay of Biscay
286 are located (i) at the base of slope of the South Armorican shelf and (ii) along the Biscay Wedge
287 Front in connection with the northern depocenter of the Landes Plateau.

288 *Interpretation*: The Aquitaine Plateau was upstream uplifted and incised by rivers
289 (Mouchené et al., 2017; Ortiz et al., 2020). All the products of erosion are transferred to the
290 deepest domains with by-pass to very low sedimentation along the modern Landes Forest
291 (Dubreuilh et al., 1995). The prograding sedimentary wedge is now located at the border of
292 the Aquitaine shelf and the two canyons (Capbreton and Cap-Ferret) alternated periods of
293 erosion and deposition (Cremer, 1983; Iglesias, 2009).

294

295 **5. Measurement of the siliciclastic sediment budget: results (fig. 7)**

296

297 In the deep-sea plain, siliciclastic volume measurements were only performed in the
298 south deep Bay of Biscay Basin, south of the Gascogne Dome Bulge, the sediment located
299 northward (Armorican Subbasin) being fed from the Loire River (fig. 1) and the Armorican
300 Massif (see 4.1). In addition, during Cenozoic times the deep-sea Bay of Biscay fan fed through
301 the Capbreton and Cap-Ferret Canyon by the sediments coming from the Aquitaine Basin is
302 progressively migrating westward (Cremer, 1983; Iglesias, 2009; Brocheray et al., 2014). This
303 is the reason why, our calculation area is evolving according to the deep-sea fan location (Figs,
304 3, 4, 5, 6).

305

306 The total amount of siliciclastic sediments (Tab. 1, Fig. 7) deposited from the Aquitaine
307 Platform to the south deep Bay of Biscay during Cenozoic times is 51 500 km^3 with an
308 uncertainty of 16 800 km^3, i.e. 33%.

309

310 The four-time intervals here defined, have not the same duration and therefore
311 siliciclastic sedimentation rates had to be used for a comparison between time intervals
312 instead of volumes (Tab. 1, fig. 7). At first order the sedimentation rates are increasing from
313 535 km^3/Myr (between 66 and 33.9 Ma) to 3150 km^3/Myr (from 5.3 to 0 Ma). Oligocene and
314 Pliocene-Pleistocene seems to be significant instants of siliciclastic sediment rates increase.

315

316 The siliciclastic sediment budget comparison (Tab. 1, fig. 7) between the onshore
317 (Aquitaine Basin) and offshore (Aquitaine shelf, Landes Plateau, south Bay of Biscay) shows a
318 shift, trough Cenozoic times, from onshore to offshore preferential accumulation since
319 Oligocene-Miocene boundary. The sediment ratio between onshore and offshore (R_{OnOff}) is (i)
320 25.3 from 66 to 33.9 Ma, (ii) 7.5 from 33.9 to 23.03 Ma, (iii) 0.18 from 23.03 to 5.3 Ma and (iv)
321 0.01 from 5.3 to 0 Ma.

322

323 **6. Discussion on the siliciclastic sediment budget**

324

325 *Volume comparison with South Pyrenean Foreland and others orogenic adjacent basins* - The
326 amount of siliciclastic sediments preserved in northern foreland is 51 500 ± 16 800 km^3 for
327 Cenozoic times. A comparison with the sediment volumes of other orogenic systems
328 supposes to get a sediment budget for both sides of the Pyrenees, i.e. including the South
329 Pyrenean Foreland basin. Several studies have been conducted for quantifying the preserved
330 sediment volumes in the South Pyrenean sink (i.e. Ebro and Valencia Basins)(Nelson, 1990;
331 Garcia-Castellanos et al., 2003; Babault et al., 2006; Filleaudeau, 2011; Arche et al., 2010;
332 Watts and Torné, 1992). The Ebro Basin has been under endoreic conditions since 36.2 Ma

333 (Costa et al., 2010) and then opened towards the Mediterranean Sea between 12 Ma and
334 7.5 Ma (Garcia-Castellanos et al., 2003; Fillon et al., 2012; Garcia-Castellanos and
335 Larrasoana, 2015). The total amount of preserved sediments in the Ebro and Valencia Basin
336 is 260 300 km^3 since 66 Myr. For a better sediment budget on both sides of the Pyrenees,
337 only the sediments coming from the mountain belt should be considered, i.e. the total
338 Cenozoic preserved sediments volumes in the Ebro basin and the Neogene for the Valencia
339 Basin. This corresponds to a range between 78 000 km^3 (Filleaudeau, 2011) and 110 000 km^3
340 ± 5000 km^3 (Garcia-Castellanos et al., 2003) in the Ebro Basin and 92 000 km^3 in the Valencia
341 Basin (Garcia-Castellanos et al., 2003). This gives a total of preserved sediments between
342 170 000 km^3 and 202 000 km^3. At the first order, this result shows a factor of four between
343 the northern retroforeland (our study) and the South Pyrenean proforeland.
344 The first-order estimation of total volume preserved in the Pyrenean adjacent basins
345 (i.e. Aquitaine Basin, Bay of Biscay, Ebro Basin, Valencia Basin) is between 220 000 km^3 and
346 250 000 km^3. The total volume of siliciclastic sediments produced by the Alps since Oligocene
347 times is of 890 000 km^3 (220 000 km^3 from the Eastern Alps and 670 000 km^3 from the western
348 ones- Kuhlemann et al., 2002) i.e. four times more than the Pyrenees. However, for larger
349 orogens the order of magnitude changes with 3.35 10^6 km^3 of sediment produced by the Rocky
350 Mountains on its continental part and stored in the Gulf of Mexico (Galloway et al., 2011) and
351 the 4.95 10^6 km^3 by the western side of the Himalaya and accumulated along of the Indus
352 Delta (Clift et al., 2006).
353
354 *Volume comparison with Pyrenean thermochronological data* – We present here some
355 volumes estimation for the Cenozoic period based on published themrochronology data in the
356 Pyrenees.

- Too few data (AFT and AHe) provide Palaeocene to early Eocene ages to obtain a consistent exhumation trend across the entire Pyrenean range.

- During the late Eocene/lower Oligocene (from 37 to 30 Ma), orogenic exhumation (> 0.5 km/Myr) is recorded in Central and Eastern Pyrenean Massif (Maladetta, Nogueres, Canigou) according to studies from Fitzgerald et al., (1999), Gibson et al., (2007), Fillon and Van der Beek, (2012) and Gunnel et al., (2009). These authors modeled an exhumation rate of 1.5 to 4 km/Myr. Considering an average of 2 km/Myr integrated over the whole area (inducing a strong assumption of a continuous constant exhumation) during the period of 35-30 Ma, the eroded volume should be of 50 000 km^3. This value is very high compared to what has been measured in the Aquitaine Basin during the same period (16 500 km^3 from base Cenozoic to base Oligocene). This volume seems therefore to supply mainly the Ebro basin with a significant increase observed at the base of Oligocene (i.e. 33.9 Ma) (Filleaudeau, 2011).

- Since middle Oligocene times, a moderate exhumation (between 0.1 and 0.5 km/Myr) is proposed by several authors in Western, Central and Eastern massifs of the Pyrenean range (DeFelipe et al., 2019; Bosch et al., 2016; Fillon et al., 2021; Fitzgerald et al., 1999; Gibson et al., 2007). An average exhumation rate of 0.25 km/Myr across the entire range provides an estimation of 17 500 km^3 for the Middle to Late Oligocene period. This volume is, like during Late Eocene/Lower Oligocene, one order of magnitude higher than what we measure in the Aquitaine Basin. This volume supply mainly the Ebro basin where the Oligocene volumes are very large (around 45 000 km^3 in Filleaudeau, 2011).

- Finally, the important increase of exhumation rate recorded in the Western Pyrenees (see Fillon et al., (2021) for the data synthesis and modelling) infers a volume estimation of 2 000 km^3 for the late Miocene period. This quantification is low compared to the volumes of preserved sediments.

We draw attention to the fact that these estimation are produces from an average of the results of modelling data done in 1D and extrapolated on a surface. These volumes based on thermochronological data are probably overestimated.

6.1. Age estimation of siliciclastic sediment flux increase from interpreted seismic data

As we mentioned earlier, the low stratigraphic resolution (Palaeocene-Eocene, Oligocene, Miocene and Pliocene-Pleistocene) is due to difficulties to propagate the high resolution age model (established in shallow marine setting in the Aquitaine Platform and Landes Plateau – Ortiz et al., 2020) across the whole seismic survey in the deep Bay of Biscay Basin and continental Aquitaine series. In order to be more precise about the age of the siliciclastic rate increase during the two key periods (Oligocene and Plio-Pleistocene) and their possible links to climatic or geodynamic event, we performed a 2D quantification on the cross section published in Ortiz et al., (2020). This quantification aims at comparing on three different locations (proximal Aquitaine platform – deep Bay of Biscay Basin – progradational wedges in between) the percentage of 2D surface (comprising sediment) normalized on their duration between each high-resolution timeline.

The figure 8 present the results and shows a refined estimate of increase at 26.0 ± 2.0 Ma for Oligocene period and 2.5 ± 0.5 Ma for Pliocene-Pleistocene period.

6.2. The 26.0 ± 2.0 Ma increase

The measured Late Oligocene (26.0 ± 2.0 Ma) siliciclastic rate increase could be explained by both a tectonic factor – the accretion of Pyrenees basal units – and a climatic factor – the icehouse-greenhouse transition and the late Oligocene warming (Zachos et al., 2001).

Tectonic - A Late Eocene to Oligocene/Miocene paroxysm of denudation (37-29 Ma central Pyrenees and 37-20 Ma western Axial Zone) is measured by the numerous thermochronological studies (see references in section 2.1) and by the dated active tectonics mainly in the Southern Pyrenees (Montsec and Sierras exteriores thrust systems associated to Orri and Rialp thrust sheets, see Munoz, 1992, Teixell, 1998, Vergés et al., 2002 and Mouthereau et al., 2014), or in the Jaca Basin cover thrust and associated Gavarnie and more frontal thrusts (Labaume et al., 2016). During late Oligocene time, the retro-foreland is affected by several truncation/erosional surfaces from 27.1 to 25.2 Ma (Ortiz et al., 2020). During this event, some syn-orogenic deposits are recycled and can be transferred to more distal sink. The observed increasing volumes and increasing export of sediment to the Bay of Biscay is thus contemporaneous with a (long) denudation paroxysm, but also with a more temporally resolved drop of preservation in the foreland which becomes less subsident and might be locally eroded and recycled. The observed modification of source to sink pattern might record combination of two processes, denudation increasing phase and cessation of subsidence in the foreland could explain the increase export toward the final sink and sedimentation rate increase observed in the western Aquitaine Platform part (fig. 4).

Climate - Few palaeoclimatological data dealing with the palaeoprecipitation record are available in the Aquitaine Basin. A palaeobotanical synthesis (Dupéron-Laudoueneix and Pons, 1985) indicate a cooling expressed by a decrease of the tropical taxon from the Eocene

to the Oligocene that corresponds to the Eocene-Oligocene global cooling event (Zachos et al., 2011). This event takes place at 33.9 Ma, thus well before the observed 26 Ma event.

The 26.0 ± 2.0 Ma increase event is contemporary with the Late Oligocene Warming, that correspond to a sustained *ca.* 6°C global warming (Zachos et al., 2001). Warming events (such as PETM) can cause sediment pulses (Foreman et al., 2012). Schlunegger and Norton, (2015) have tested this increase hypothesis in the Alpine Foreland Basin. They focus on the Napf megafan sedimentary evolution in the Alpine foothills during this period of sudden warming. As in our study the period is also a time of increasing exhumation phase in the Alpine mountain (Schmid et al., 1996). They didn't observe remarkable shift in the water discharge, and they ruled out the hypothesis of sediment rate increase due to the Late Oligocene warming but linked it to tectonic process.

In our case, the Late Oligocene (26.0 ± 2.0 Ma) siliciclastic rate increase is linked to the high erosion rates and lower preservation in the Aquitaine Platform controlled by the orogenic tectonic processes. This increase is also registered in the Ebro basin (Filleaudeau, 2011).

6.3. The 2.5 ± 0.5 Ma increase and the long-term volume increase

The change in the rate of siliciclastic sediment supply during Plio-Pleistocene (at 2.5 ± 0.5 Ma) is significant (fig. 8) and sharply accentuates the overall increasing rate trend through Cenozoic times. This confirms for this area, the Hay's curve (Hay et al., 1989, 1990; Wold et Hay, 1990) showing a world-scale increase of the siliciclastic fluxes up to today, interpreted by Molnar (Molnar and England, 1990; Molnar, 2004) as the consequence of the global Earth cooling during Plio-Pleistocene times. Herman et al., (2013) further suggest a Plio-Pleistocene (at around 6 Ma) increase in erosion rates and with an acceleration at around 2 Ma that they

attribute to the global cooling Pliocene and Pleistocene episodes that enhanced erosion in mountainous glaciated area.

Onshore, the most sensible low-temperature thermochronological data, ((U-TH)/He and Fission tracks on apatites) do not show any Pliocene increase of denudation either in the Pyrenees Mountains (e.g. Bosch et al., 2016) or in the French Massif central (T. François, personal communications). The youngest cooling episode is recorded at around 10 Ma (Late Miocene) in the western axial zone and no basin erosion > 1.5 km could be retrieved in the Aquitaine Basin for the last 20 Myrs (Fillon et al., 2021), except in easternmost Aquitaine Basin (Corbières area) Al Reda et al., (2021) althought this denudation event is temporally poorly resolved between 20 and 5 Ma, this event is attributed by the authors to early Miocene and opening of the Gulf o Lion.

With these observations, several hypothesis have yet to be tested: (1) a climate effect on the intensity and pattern of erosion, with the effect of glaciations and change of the pattern of erosion, from widely distributed before 5.3 Ma to localized in valleys after with a greater climate effect from 2 Ma, which could be associated to (2) an “underestimated” significant re-erosion of previously deposited sediments in the Aquitaine Basin (“cannibalization”) and (3) lateral supply of sediments from other sources in the deep-sea domain under the action of deep-sea currents (Le Danois Contourite Depositional System due to Mediterranean Outflow Water, Van Rooij et al., 2010). Moreover, Pliocene-Pleistocene evolution of the Aquitaine Platform records a two steps evolution, the emplacement of megafans with the most striking one i.e. Lannemezan megafan starting during Messinian up to Uppermost Pliocene (Ortiz et al., 2020). This megafan mainly source by the Neste River is dissected during Late Quaternary (at or before 300 ka, Mouchené et al., 2017). This indicates a shift from a sedimentation phase

474 to an incision phase, that takes place between 2.6 Ma and 300 ka. This supports the hypothesis
475 of recycling by erosion of previous deposits sediments in the Aquitaine Platform.
476 Although glaciations is well documented during Late Quaternary in the Pyrenees
477 (Calvet et al., 2011; Delmas et al., 2008), their importance in terms of sedimentary budget is
478 still not quantified. Identified glacial remnants are restricted to the upper part of the valleys
479 and mostly confined in the mountains belts (Delmas et al., 2011). The preservation over large
480 areas of preglacial flat surfaces in the high chain (Bosch et al., 2016) claim for erosion localized
481 mainly in glacial valleys. This supports the hypothesis of a more localized erosion in the
482 mountain valleys.
483
484
485 **6.4. Sediment budget evolution between onshore and offshore**
486
487 The change of the sediment ratio between onshore and offshore (R_{OnOff}) from 25.3 (66
488 to 33.9 Ma) to 0.01 (5.3 to 0 Ma) has to be related to the general evolution of the two basins
489 as summarized in item 2.2. This drastic change of ratio in favour of the "ultimate sink" is in
490 line with the synthesis of Hinderer, 2012.
491 • The first interval (66.0-33.9 Ma) spans a long period of time and several steps of the
492 orogeny. A first phase (66-56 Ma) of relatively quiescent with very low relief in the
493 mountain belt and siliciclastic input, a second phase (56-33.9 Ma) that correspond to
494 progressive mountain building with increasing relief and erosion. At around 40 Ma,
495 deformation propagate in the foredeep and segmented the foredeep. During this entire
496 period, accommodation space created by the flexure was large enough to trap siliciclastic

sediments coming from the incipient mountain belt. This may explain the general trend between 66 and 33.9 Ma.

- The second period (33.9-23.03 Ma) also spans different periods, paroxysm of denudation in the Mountain belt, while in the Aquitaine Platform, two periods are deciphered, a first period of accumulation and deformation (up to 25.2 Ma) and a second with a decrease of subsidence and increase of export to the distal sink (since 25.2 Ma). As a consequence, since 25.2 Ma, siliciclastic supply is too important compare to the accommodation space creation and the sediments are transferred to the progradational wedges in the Aquitaine platform. This explains the trend during Oligocene and particularly since 25.2.
- During the post-orogenic period, first the Aquitaine platform subsidence drastically decreased (25.2-10.6 Ma) and second this domain was partly uplifted (10.6-0 Ma). This favored the sediment export to the deep-sea domain, first poorly balanced (R_{OnOff} at 0.18 – map 23.03-5.3 Ma) and then unbalanced (R_{OnOff} at 0.01 - map 5.3-0 Ma).

7. Conclusion

Our objective was to measure the siliciclastic sediment volumes and rates of a retro-foreland basin and its lateral deep equivalent, during the end tectonic and topographic evolution of the Pyrenees mountain belt.

(1) The amount of sediments is of 51 500 ± 16 800 km^3 for the Cenozoic.

(2) The siliciclastic sediment rate curve during Cenozoic shows two major increase around 26.0 and 2.5 Ma. This last one is a major increase. This is in agreement with the world-scale trend of Hay et al. (1989), expected of climatic origin by Molnar and England (1990).

The 26.0 Ma increase is clearly related to the exhumation of the Pyrenees of tectonic origin. The discussion on the major 2.5 Ma episode is still open.

(3) The mass balance between the Aquitaine Platform and the deepest domains (Landes Plateau, Bay of Biscay) change through time in favour to the deep domain. This might be explained by the ratio between subsidence created accommodation space and the produced siliciclastic sediments by the mountain belt on the platform. This confirms and quantifies the stratigraphic model of sink preservation proposed by Ortiz et al. (2020). This also suggests the sediment accumulation in the deep part of the margin is only controlled by the accommodation/sedimentation balance on the platform.

Data Availability Statement

Research data are not shared

References

Allen, P.A., Allen, J.R., 2013. Basin analysis: Principles and application to petroleum play assessment. John Wiley & Sons.

Al Reda, S. M., Barbarand, J., Gautheron, C., Lasseur, E., Loget, N., Pinna-Jamme, R., & Briais, J., 2021. Thermal record of the building of an orogen in the retro-foreland basin: Insight from basement and detrital thermochronology in the eastern Pyrenees and the north Pyrenean basin (France). *Basin Research*, **33**(5), 2763-2791.

Angrand, P., Ford, M., Watts, A.B., 2018. Lateral variations in foreland flexure of a rifted continental margin: The Aquitaine Basin (SW France). *Tectonics* **37**, 430–449.

543 Arche, A., Evans, G., & Clavell, E., 2013. Some considerations on the initiation of the present
544 SE Ebro river drainage system: Post-or pre-Messinian?. *Ene*, **13**, 10.

545 Armitage, J.J., Allen, P.A., Burgess, P.M., Hampson, G.J., Whittaker, A.C., Duller, R.A.,
546 Michael, N.A., 2015. Sediment transport model for the Eocene Escanilla sediment-
547 routing system: Implications for the uniqueness of sequence stratigraphic architectures.
548 *J. Sediment. Res.* **85**, 1510–1524.

549 Babault, J., Loget, N., Van Den Driessche, J., Castelltort, S., Bonnet, S., & Davy, P., 2006.
550 Did the Ebro basin connect to the Mediterranean before the Messinian salinity
551 crisis?. *Geomorphology*, **81**(1-2), 155-165.

552 Babault, J., Van Den Driessche, J., Bonnet, S., Castelltort, S., & Crave, A., 2005. Origin of
553 the highly elevated Pyrenean peneplain. *Tectonics*, **24**(2).

554 Beamud, E., Muñoz, J. A., Fitzgerald, P. G., Baldwin, S. L., Garcés, M., Cabrera, L., &
555 Metcalf, J. R., 2011. Magnetostratigraphy and detrital apatite fission track
556 thermochronology in syntectonic conglomerates: constraints on the exhumation of the
557 South-Central Pyrenees. *Basin Research*, **23**(3), 309-331.

558 Beaumont, C., 1981. Foreland basins. *Geophys. J. Int.* **65**, 291–329.

559 Beaumont, C., Fullsack, P., Hamilton, J., 1992. Erosional control of active compressional
560 orogens. In: McClay, K. (Ed.), Thrust Tectonics. *Chapman & Hall, London, UK*, pp.1–18.

561 Bosch, G. V, Teixell, A., Jolivet, M., Labaume, P., Stockli, D., Domènech, M., Monié, P.,
562 2016. Timing of Eocene--Miocene thrust activity in the Western Axial Zone and
563 Chainons Béarnais (west-central Pyrenees) revealed by multi-method thermochronology.
564 *Comptes Rendus Geosci.* **348**, 246–256.

565 Bosch, G. V., Van Den Driessche, J., Babault, J., Robert, A., Carballo, A., Le Carlier, C., ... &
566 Baudin, T., 2016. Peneplanation and lithosphere dynamics in the Pyrenees. *Comptes*
567 *Rendus Géoscience*, **348**(3-4), 194-202.

568 Braun, J., 2003. Pecube: A new finite-element code to solve the 3D heat transport equation
569 including the effects of a time-varying, finite amplitude surface topography. *Computers*
570 *& Geosciences*, **29**(6), 787-794.

571 Braun, J., Van Der Beek, P., Valla, P., Robert, X., Herman, F., Glotzbach, C., ... & Prigent,
572 C., 2012. Quantifying rates of landscape evolution and tectonic processes by
573 thermochronology and numerical modeling of crustal heat transport using
574 PECUBE. *Tectonophysics*, **524**, 1-28.

575 Brocheray, S., Cremer, M., Zaragosi, S., Schmidt, S., Eynaud, F., Rossignol, L., & Gillet, H.
576 2014. 2000 years of frequent turbidite activity in the Capbreton Canyon (Bay of
577 Biscay). *Marine Geology*, **347**, 136-152.

578 Brunet, M. F., 1984. Subsidence history of the Aquitaine basin determined from subsidence
579 curves. *Geological Magazine*, **121**(5), 421-428.

580 Brunet, M. F., 1994. Subsidence in the Parentis Basin (Aquitaine, France): Implications of the
581 thermal evolution. In *Hydrocarbon and petroleum geology of France* (pp. 187-198).
582 Springer, Berlin, Heidelberg.

583 Burbank, D. W., & Anderson, R. S., 2009. *Tectonic geomorphology*. John Wiley & Sons.

584 Calvet, M., Delmas, M., Gunnell, Y., Braucher, R., & Bourlès, D., 2011. Recent advances in
585 research on Quaternary glaciations in the Pyrenees. *Developments in Quaternary*
586 *Sciences*, **15**, 127-139.

Clerc, C., Lagabrielle, Y., Labaume, P., Ringenbach, J.-C., Vauchez, A., Nalpas, T., Bousquet, R., Ballard, J.-F., Lahfid, A., Fourcade, S., 2016. Basement--Cover decoupling and progressive exhumation of metamorphic sediments at hot rifted margin. Insights from the Northeastern Pyrenean analog. *Tectonophysics* **686**, 82–97.

Clerc, C., Lagabrielle, Y., Neumaier, M., Reynaud, J. Y., & de Saint Blanquat, M., 2012. Exhumation of subcontinental mantle rocks: evidence from ultramafic-bearing clastic deposits nearby the Lherz peridotite body, French Pyrenees. *Bulletin de la Société géologique de France*, **183**(5), 443-459.

Clift, P.D., 2006. Controls on the erosion of Cenozoic Asia and the flux of clastic sediment to the ocean. *Earth Planet. Sci. Lett.* **241**, 571–580.

Costa, E., Garces, M., López-Blanco, M., Beamud, E., Gómez-Paccard, M., & Larrasoaña, J. C., 2010. Closing and continentalization of the South Pyrenean foreland basin (NE Spain): magnetochronological constraints. *Basin Research*, **22(6)**, 904-917.

Cremer, M., 1983. Approches sédimentologique et géophysique des accumulations turbiditiques: l'éventail profond du Cap-Ferret (Golfe de Gascogne), la série des grès d'Annot (Alpes-de-Haute-Provence) 1 Thèse, Université de Bordeaux

DeFelipe, I., Pedreira, D., Pulgar, J. A., Van der Beek, P. A., Bernet, M., & Pik, R., 2019. Unraveling the Mesozoic and Cenozoic tectonothermal evolution of the eastern Basque-Cantabrian zone–western Pyrenees by low-temperature thermochronology. *Tectonics*, **38(9)**, 3436-3461.

609 Delmas, M., Gunnell, Y., Braucher, R., Calvet, M., & Bourlès, D., 2008. Exposure age
610 chronology of the last glaciation in the eastern Pyrenees. *Quaternary Research*, **69**(2), 231-
611 241.
612 Delmas, M., Calvet, M., Gunnell, Y., Braucher, R., & Bourlès, D., 2011. Palaeogeography
613 and 10Be exposure-age chronology of Middle and Late Pleistocene glacier systems in the
614 northern Pyrenees: implications for reconstructing regional palaeoclimates. *Palaeogeography,*
615 *Palaeoclimatology, Palaeoecology*, **305**(1-4), 109-122.
616
617 Desegaulx, P. A. S. C. A. L., & Brunet, M. F., 1990. Tectonic subsidence of the Aquitaine
618 basin since Cretaceous times. *Bulletin de la Société géologique de France*, **6**(2), 295-306.
619
620 Dubreuilh, J., Capdeville, J.P., Farjanel, G., Karnay, G., Platel, J.P., Simon-Coinçon, R.,
621 1995. Dynamique d'un comblement continental néogène et quaternaire: l'exemple du bassin
622 d'Aquitaine. *Géol. France* 3–26.
623
624 Ducoux, M., Jolivet, L., Callot, J. P., Aubourg, C., Masini, E., Lahfid, A., ... & Baudin, T.,
625 2019. The Nappe des Marbres unit of the Basque-Cantabrian Basin: the tectono-thermal
626 evolution of a fossil hyperextended rift basin. *Tectonics*, **38**(11), 3881-3915.
627
628 Ducoux, M., Jolivet, L., Cagnard, F., & Baudin, T., 2021. Basement-cover decoupling during
629 the inversion of a hyperextended basin: Insights from the Eastern Pyrenees. *Tectonics*,
630 e2020TC006512.

631 Dupéron-Laudoueneix, M., Pons, D., 1985. Nouvelle étude de Mesembrioxylon libanoticum
632 Edwards (Conifère du Mésozoïque supérieur) ; intérêts paléogéographique,
633 biostratigraphique et paléoclimatique. *Plant Biosyst.* **119**, 151–166.

Einsele, G., 2000. *Sedimentary basins: evolution, facies, and sediment budget*. Springer Science & Business Media.

England, P., 1981. Metamorphic pressure estimates and sediment volumes for the Alpine orogeny: an independent control on geobarometers? *Earth Planet. Sci. Lett.* **56**, 387–397.

Fabriès, J., Lorand, J. P., Bodinier, J. L., & Dupuy, C., 1991. Evolution of the upper mantle beneath the Pyrenees: evidence from orogenic spinel lherzolite massifs. *Journal of Petrology*, 2, 55-76.

Fabriès, J., Lorand, J. P., & Bodinier, J. L., 1998. Petrogenetic evolution of orogenic lherzolite massifs in the central and western Pyrenees. *Tectonophysics*, **292**(1-2), 145-167.

Fillon, C., van der Beek, P., 2012. Post-orogenic evolution of the southern Pyrenees: Constraints from inverse thermo-kinematic modelling of low-temperature thermochronology data. *Basin Res.* **24**, 418–436.

Fillon, C., Pedreira, D., Van Der Beek, P.A., Huismans, R.S., Barbero, L., Pulgar, J.A., 2016. Alpine exhumation of the central Cantabrian mountains, northwest Spain. *Tectonics* **35**, 339–356.

Fillon, C., Mouthereau, F., Calassou, S., Pik, R., Bellahsen, N., Gautheron, C., ... & van der Beek, P., 2021. Post-orogenic exhumation in the western Pyrenees: evidence for extension driven by pre-orogenic inheritance. *Journal of the Geological Society*, **178**(2).

Fitzgerald, P.G., Muñoz, J.A., Coney, P.J., Baldwin, S.L., 1999. Asymmetric exhumation across the Pyrenean orogen: implications for the tectonic evolution of a collisional orogen. *Earth Planet. Sci. Lett.* **173**, 157–170.

Ford, M., Hemmer, L., Vacherat, A., Gallagher, K., & Christophoul, F., 2016. Retro-wedge foreland basin evolution along the ECORS line, eastern Pyrenees, France. *Journal of the Geological Society*, **173**(3), 419-437.

Foreman, B. Z., Heller, P. L., & Clementz, M. T., 2012. Fluvial response to abrupt global warming at the Palaeocene/Eocene boundary. *Nature*, **491**(7422), 92-95.

Gallagher, K., Charvin, K., Nielsen, S., Sambridge, M., & Stephenson, J., 2009. Markov chain Monte Carlo (MCMC) sampling methods to determine optimal models, model resolution and model choice for Earth Science problems. *Marine and Petroleum Geology*, **26**(4), 525-535.

Gallastegui, J., Pulgar, J.A., Gallart, J., 2002. Initiation of an active margin at the North Iberian continent-ocean transition. *Tectonics* **21**, 11–15.

Galloway, W.E., Whiteaker, T.L., Ganey-Curry, P., 2011. History of Cenozoic North American drainage basin evolution, sediment yield, and accumulation in the Gulf of Mexico basin. *Geosphere* **7**, 938–973.

Galloway, W.E., Williams, T.A., 1991. Sediment accumulation rates in time and space: Paleogene genetic stratigraphic sequences of the northwestern Gulf of Mexico basin. *Geology* **19**, 986–989.

Garcia-Castellanos, D., Vergés, J., Gaspar-Escribano, J., & Cloetingh, S., 2003. Interplay between tectonics, climate, and fluvial transport during the Cenozoic evolution of the Ebro Basin (NE Iberia). *Journal of Geophysical Research: Solid Earth*, **108**(B7).

Garcia-Castellanos, D., & Larrasoaña, J. C., 2015. Quantifying the post-tectonic topographic evolution of closed basins: The Ebro basin (northeast Iberia). *Geology*, **43(8**), 663-666.

678 Garzanti, E., 2019. The Himalayan Foreland Basin from collision onset to the present: A
679 sedimentary–petrology perspective. *Geological Society, London, Special*
680 *Publications*, **483(1)**, 65-122.

681 Gibson, M., Sinclair, H. D., Lynn, G. J., & Stuart, F. M., 2007. Late-to post-orogenic
682 exhumation of the Central Pyrenees revealed through combined thermochronological
683 data and modelling. *Basin Research*, **19(3)**, 323-334.

684 Gómez, M., Vergés, J., Riaza, C., 2002. Inversion tectonics of the northern margin of the
685 Basque Cantabrian Basin. *Bull. la Société géologique Fr.* **173**, 449–459.

686 Goodbred Jr, S. L., & Kuehl, S. A., 2000. The significance of large sediment supply, active
687 tectonism, and eustasy on margin sequence development: Late Quaternary stratigraphy
688 and evolution of the Ganges–Brahmaputra delta. *Sedimentary Geology*, **133(3-4)**, 227-
689 248.

690 Guillocheau, F., Brault, N., Thomas, E., Barbarand, J., Bonnet, S., Bourquin, S., Estéoule-
691 Choux, J., Guennoc, P., Menier, D., Neraudeau, D., Proust, J.-N., Wyns, R., 2003. Histoire
692 géologique du Massif armoricain depuis 140 Ma (Crétacé-Actuel). *Bulletin d'Information des*
693 *Géologues du Bassin de Paris*, **40(1)**, 13-28.
694 Guillocheau, F., Rouby, D., Robin, C., Helm, C., Rolland, N., Carlier, L. E., Braun, J. (2012).
695 Quantification and causes of the terrigeneous sediment budget at the scale of a continental
696 margin: A new method applied to the Namibia-South Africa margin. *Basin Research*, ***24***, 3–
697 30.
698 Gunnell, Y., Calvet, M., Brichau, S., Carter, A., Aguilar, J. P., & Zeyen, H., 2009. Low long-
699 term erosion rates in high-energy mountain belts: Insights from thermo-and biochronology in
700 the Eastern Pyrenees. *Earth and Planetary Science Letters*, **278(3-4)**, 208-218.

Hay, W.W., Shaw, C.A., Wold, C.N., 1989. Mass-balanced paleogeographic reconstructions. *Geol. Rundschau* **78**, 207–242.

Hay, W.W., Wold, C.N., 1990. Relation of selected mineral deposits to the mass/age distribution of Phanerozoic sediments. *Geol. Rundschau* **79**, 495–512.

Herman, F., Seward, D., Valla, P. G., Carter, A., Kohn, B., Willett, S. D., & Ehlers, T. A., 2013. Worldwide acceleration of mountain erosion under a cooling climate. *Nature*, **504**(7480), 423-426.

Herman, F., Champagnac, J.-D., 2016. Plio-Pleistocene increase of erosion rates in mountain belts in response to climate change. *Terra Nov.* **28**, 2–10.

Hinderer, M., 2012. From gullies to mountain belts: a review of sediment budgets at various scales. *Sedimentary Geology*, **280**, 21-59.

Iglesias, J., 2009. Sedimentation on the cantabrian continental margin from late oligocene to quaternary.

Jammes, S., Manatschal, G., Lavier, L., & Masini, E., 2009. Tectonosedimentary evolution related to extreme crustal thinning ahead of a propagating ocean: Example of the western Pyrenees. *Tectonics*, **28**(4).

Jolivet, M., Labaume, P., Monié, P., Brunel, M., Arnaud, N., & Campani, M., 2007. Thermochronology constraints for the propagation sequence of the south Pyrenean basement thrust system (France-Spain). *Tectonics*, **26**(5).

Ketcham, R. A., 2005. Forward and inverse modeling of low-temperature thermochronometry data. *Reviews in mineralogy and geochemistry*, **58**(1), 275-314.

722 Kuhlemann, J., Frisch, W., Székely, B., Dunkl, I., Kázmér, M., 2002. Post-collisional
723 sediment budget history of the Alps: tectonic versus climatic control. *Int. J. Earth Sci.*
724 **91**, 818–837.

725 Kuhlemann, J., 2000. Post-collisional sediment budget of circum-Alpine basins (Central
726 Europe). *Mem. Sci. Geol. Padova* **52**, 1–91.

727 Labaume, P., Meresse, F., Jolivet, M., & Teixell, A., 2016. Exhumation sequence of the
728 basement thrust units in the west-central Pyrenees. Constraints from apatite fission track
729 analysis. *Geogaceta*, **60**, 11-14.

730 Lagabrielle, Y., & Bodinier, J. L., 2008. Submarine reworking of exhumed subcontinental
731 mantle rocks: field evidence from the Lherz peridotites, French Pyrenees. *Terra*
732 *Nova*, **20**(1), 11-21.

733 Lagabrielle, Y., Labaume, P., de Saint Blanquat, M., 2010. Mantle exhumation, crustal
734 denudation, and gravity tectonics during Cretaceous rifting in the Pyrenean realm (SW
735 Europe): Insights from the geological setting of the lherzolite bodies. *Tectonics* **29**.

736 Leroux, E., Rabineau, M., Aslanian, D., Gorini, C., Molliex, S., Bache, F., & Suc, J. P., 2017.
737 High-resolution evolution of terrigenous sediment yields in the Provence Basin during
738 the last 6 Ma: relation with climate and tectonics. *Basin Research*, **29**(3), 305-339.

739 Macchiavelli, C., Vergés, J., Schettino, A., Fernàndez, M., Turco, E., Casciello, E., Torne, M.,
740 Pierantoni, P.P., Tunini, L., 2017. A new southern North Atlantic isochron map: Insights
741 into the drift of the Iberian plate since the Late Cretaceous. *J. Geophys. Res. Solid Earth*
742 **122**, 9603–9626.

743 Masini, E., Manatschal, G., Tugend, J., Mohn, G., Flament, J.-M., 2014. The tectono-
744 sedimentary evolution of a hyper-extended rift basin: the example of the Arzacq--
745 Mauléon rift system (Western Pyrenees, SW France). *Int. J. Earth Sci.* **103**, 1569–1596.

746 Maurel, O., Monie, P., Pik, R., Arnaud, N., Brunel, M., & Jolivet, M., 2008. The Meso-
747 Cenozoic thermo-tectonic evolution of the Eastern Pyrenees: an 40 Ar/39 Ar fission
748 track and (U–Th)/He thermochronological study of the Canigou and Mont-Louis
749 massifs. *International Journal of Earth Sciences*, **97(3)**, 565-584.

750 Metcalf, J. R., Fitzgerald, P. G., Baldwin, S. L., & Muñoz, J. A., 2009. Thermochronology of
751 a convergent orogen: Constraints on the timing of thrust faulting and subsequent
752 exhumation of the Maladeta Pluton in the Central Pyrenean Axial Zone. *Earth and*
753 *Planetary Science Letters*, **287(3-4)**, 488-503.

754 Métivier, F., Gaudemer, Y., Tapponnier, P., Klein, M., 1999. Mass accumulation rates in Asia
755 during the Cenozoic. *Geophys. J. Int.* **137**, 280–318.

756 Michael, N.A., Whittaker, A.C., Allen, P.A., 2013. The functioning of sediment routing
757 systems using a mass balance approach: Example from the Eocene of the southern
758 Pyrenees. *J. Geol.* **121**, 581–606.

759 Michael, N.A., Carter, A., Whittaker, A.C., Allen, P.A., 2014. Erosion rates in the source
760 region of an ancient sediment routing system: Comparison of depositional volumes with
761 thermochronometric estimates. *J. Geol. Soc. London.* **171**, 401–412.

762 Michael, N.A., Whittaker, A.C., Carter, A., Allen, P.A., 2014. Volumetric budget and grain-
763 size fractionation of a geological sediment routing system: Eocene Escanilla Formation,
764 south-central Pyrenees. *Bull. Geol. Soc. Am.* **126**, 585–599.

765 Molnar, P., 2004. Late Cenozoic increase in accumulation rates of terrestrial sediment: How
766 might climate change have affected erosion rates? *Annu. Rev. Earth Planet. Sci.* **32**, 67–
767 89.

768 Molnar, P., England, P., 1990. Late Cenozoic uplift of mountain ranges and global climate
769 change: chicken or egg? *Nature* **346**, 29–34.

770 Molnar, P., Lyon-Caen, H., 1988. Some simple physical aspects of the support, structure, and
771 evolution of mountain belts. *Process. Cont. lithospheric Deform.* **218**, 179–207.

772 Mouchené, M., van der Beek, P., Mouthereau, F., & Carcaillet, J., 2017. Controls on
773 Quaternary incision of the Northern Pyrenean foreland: Chronological and
774 geomorphological constraints from the Lannemezan megafan, SW
775 France. *Geomorphology*, **281**, 78-93.

776 Mouthereau, F., Filleaudeau, P. Y., Vacherat, A., Pik, R., Lacombe, O., Fellin, M. G., ... &
777 Masini, E., 2014. Placing limits to shortening evolution in the Pyrenees: Role of margin
778 architecture and implications for the Iberia/Europe convergence. *Tectonics*, **33(12)**,
779 2283-2314.

780 Muñoz, J. A., 1992. Evolution of a continental collision belt: ECORS-Pyrenees crustal
781 balanced cross-section. In *Thrust tectonics* (pp. 235-246). Springer, Dordrecht.

782 Najman, Y., & Garzanti, E., 2000. Reconstructing early Himalayan tectonic evolution and
783 paleogeography from Tertiary foreland basin sedimentary rocks, northern
784 India. *Geological Society of America Bulletin*, **112(3)**, 435-449.

785 Nelson, C. H., 1990. Estimated post-Messinian sediment supply and sedimentation rates on
786 the Ebro continental margin, Spain. *Marine Geology*, *95*(3-4), 395-418.

Ortiz, A., Guillocheau, F., Lasseur, E., Briais, J., Robin, C., Serrano, O., Fillon, C., 2020. Sediment routing system and sink preservation during the post-orogenic evolution of a retro-foreland basin: The case example of the North Pyrenean (Aquitaine, Bay of Biscay) Basins. *Mar. Pet. Geol.* **112**, 104085.

Pedreira, D., Afonso, J.C., Pulgar, J.A., Gallastegui, J., Carballo, A., Fernàndez, M., Garcia-Castellanos, D., Jiménez-Munt, I., Semprich, J., Garcia-Moreno, O., 2015. Geophysical-petrological modeling of the lithosphere beneath the Cantabrian Mountains and the North-Iberian margin: Geodynamic implications. *Lithos* **230**, 46–68.

Roest, W.R., Srivastava, S.P., 1991. Kinematics of the plate boundaries between Eurasia, Iberia, and Africa in the North Atlantic from the Late Cretaceous to the present. *Geology* **19**, 613–616.

Roure, F., Choukroune, P., Berastegui, X., Munoz, J. A., Villien, A., Matheron, P., . & Deramond, J., 1989. ECORS deep seismic data and balanced cross sections: Geometric constraints on the evolution of the Pyrenees. *Tectonics*, **8(**1), 41-50.

Saspiturry, N., Razin, P., Baudin, T., Serrano, O., Issautier, B., Lasseur, E., Allanic, C., Thinon, I., Leleu, S., 2019. Symmetry vs. asymmetry of a hyper-thinned rift: example of the Mauléon Basin (Western Pyrenees, France). *Mar. Pet. Geol.* **104**, 86–105.

Schettino, A., Turco, E., 2011. Tectonic history of the western Tethys since the Late Triassic. *Bulletin*, **123**(1-2), 89–105.

Schlunegger, F., Melzer, J., & Tucker, G., 2001. Climate, exposed source-rock lithologies, crustal uplift and surface erosion: a theoretical analysis calibrated with data from the

Alps/North Alpine Foreland Basin system. *International Journal of Earth Sciences*, **90(3)**, 484-499.

Schlunegger, F., & Mosar, J., 2011. The last erosional stage of the Molasse Basin and the Alps. *International Journal of Earth Sciences*, **100**(5), 1147-1162.

Schlunegger, F., & Norton, K. P., 2015. Climate vs. tectonics: the competing roles of Late Oligocene warming and Alpine orogenesis in constructing alluvial megafan sequences in the North Alpine foreland basin. *Basin research*, **27**(2), 230-245.

Schmid, S. M., Pfiffner, O. A., Froitzheim, N., Schönborn, G., & Kissling, E., 1996. Geophysical-geological transect and tectonic evolution of the Swiss-Italian Alps. *Tectonics*, **15**(5), 1036-1064.

Serrano, O., 2001. Le Crétacé Supérieur-Paléogène du Bassin Compressif Nord-Pyrénéen (Bassin de l'Adour). Sédimentologie, Stratigraphie, Géodynamique. Université Rennes 1.

Serrano, O., Guillocheau, F., & Leroy, E., 2001. Évolution du bassin compressif Nord-Pyrénéen au Paléogène (bassin de l'Adour): contraintes stratigraphiques. *Comptes Rendus de l'Académie des Sciences-Series IIA-Earth and Planetary Science*, **332**(1), 37-44.

Sinclair, H.D., Gibson, M., Naylor, M., Morris, R.G., 2005. Asymmetric growth of the Pyrenees revealed through measurement and modeling of orogenic fluxes. *Am. J. Sci.* **305**, 369–406.

828 Sztrákos, K., Gély, J. P., Blondeau, A., & Muller, C., 1998. L'Eocène du Bassin sud-aquitain:
829 lithostratigraphie, biostratigraphie et analyse séquentielle. *Géologie de la France*, (4),
830 57-105.

831 Sztrákos, K., & Steurbaut, E., 2017. Révision lithostratigraphique et biostratigraphique de
832 l'Oligocène d'Aquitaine occidentale (France). *Geodiversitas*, **39**(4), 741-781.

833

834 Teixell, A., 1998. Crustal structure and orogenic material budget in the west central
835 Pyrenees. *Tectonics*, **17(3)**, 395-406.

836 Ternois, S., Odlum, M., Ford, M., Pik, R., Stockli, D., Tibari, B., Vacherat, A., Bernard, V.,
837 2019. Thermochronological evidence of early orogenesis, eastern Pyrenees, France.
838 *Tectonics* **38**, 1308–1336.

839 Thinon, I., 1999. Structure profonde de la marge nord-Gascogne et du bassin armoricain.
840 Brest.

841 Thinon, I., Fidalgo-González, L., Réhault, J.-P., Olivet, J.-L., 2001. Déformations
842 pyrénéennes dans le golfe de Gascogne. *Comptes Rendus l'Académie des Sci. IIA-Earth*
843 *Planet. Sci.* **332**, 561–568.

844 Tugend, J., Manatschal, G., Kusznir, N. J., Masini, E., Mohn, G., & Thinon, I., 2014.
845 Formation and deformation of hyperextended rift systems: Insights from rift domain
846 mapping in the Bay of Biscay-Pyrenees. *Tectonics*, **33**(7), 1239-1276.

Vacherat, A., Mouthereau, F., Pik, R., Bernet, M., Gautheron, C., Masini, E., ... & Lahfid, A., 2014. Thermal imprint of rift-related processes in orogens as recorded in the Pyrenees. *Earth and Planetary Science Letters*, **408**, 296-306.

Vacherat, A., Mouthereau, F., Pik, R., Bellahsen, N., Gautheron, C., Bernet, M., ... & Radal, J., 2016. Rift-to-collision transition recorded by tectonothermal evolution of the northern Pyrenees. *Tectonics*, **35(4)**, 907-933.

Van Rooij, D., Iglesias, J., Hernández-Molina, F.J., Ercilla, G., Gomez-Ballesteros, M., Casas, D., Llave, E., De Hauwere, A., Garcia-Gil, S., Acosta, J., others, 2010. The Le Danois Contourite Depositional System: interactions between the Mediterranean outflow water and the upper Cantabrian slope (North Iberian margin). *Mar. Geol.* **274**, 1–20.

Vergés, J., Fernàndez, M., & Martìnez, A., 2002. The Pyrenean orogen: pre-, syn-, and post-collisional evolution. *Journal of the Virtual Explorer*, **8**, 55-74.

Waldner, M., Bellahsen, N., Mouthereau, F., Bernet, M., Pik, R., Rosenberg, C. L., & Balvay, M., 2021. Central Pyrenees mountain building: constraints from new LT thermochronological data from the Axial Zone. *Tectonics*, e2020TC006614.

Watts, A. B., & Torné, M., 1992. Crustal structure and the mechanical properties of extended continental lithosphere in the Valencia trough (western Mediterranean). *Journal of the Geological Society*, **149(5)**, 813-827.

Watts, A.B., 2001. Isostasy and Flexure of the Lithosphere. *Cambridge University Press*.

Willett, S.D., 1999. Orogeny and orography: the effects of erosion on the structure of mountain belts. *J. Geophys. Res., Solid Earth* **104** (B12), 28957–28981.

Whipple, K.X., 2009. The influence of climate on the tectonic evolution of mountain belts. *Nat. Geosci.* **2**, 97–104.

Whitchurch, A. L., Carter, A., Sinclair, H. D., Duller, R. A., Whittaker, A. C., & Allen, P. A., 2011. Sediment routing system evolution within a diachronously uplifting orogen: Insights from detrital zircon thermochronological analyses from the South-Central Pyrenees. *American Journal of Science*, **311**(5), 442-482.

Wold, C.N., Hay, W.W., 1990. Estimating ancient sediment fluxes. *Am. J. Sci.* **290**, 1069–1089.

Zachos, J., Pagani, M., Sloan, L., Thomas, E., Billups, K., 2001. Trends, rhythms, and aberrations in global climate 65 Ma to present. *Science* **292**, 686–693.

882 **Table 1 caption:** Siliciclastic sediment volumes and rates values, with the uncertainties

Accumulated solid volumes, rates and associated variance for the Aquitaine Basin

Time interval	(Ma)	Volume (× 1 km^3)	σ	Rate (× 1 km^3 / Myr)	σ
Pliocene - Pleistocene	5.33 - 0	228.6	± 10.8	43.1	± 2.0
Aquitanian - Messinian	23.03 - 5.33	1 370.3	± 385.2	77.2	± 21.7
Rupelian - Chattian	33.9 - 23.03	7 894.7	± 1 949.9	726.2	± 179.3
Danian - Priabonian	66 - 33.9	16 545.6	± 5 563.1	515.4	± 173.3

Accumulated solid volumes, rates and associated variance for the southern Bay of Biscay

Time interval	(Ma)	Volume (× 1 km^3)	σ	Rate (× 1 km^3 / Myr)	σ
Pliocene - Pleistocene	5.33 - 0	16 445.0	± 5 929.1	3 084.2	± 1 111.9
Aquitanian - Messinian	23.03 - 5.33	7 301.3	± 2 231.5	411.8	± 125.9
Rupelian - Chattian	33.9 - 23.03	1 043.7	± 351.8	96.0	± 32.4
Danian - Priabonian	66 - 33.9	652.7	± 352.0	20.6	± 11.1

Accumulated solid volumes, rates and associated variance for the whole basins

Time interval	(Ma)	Volume (× 1 km^3)	σ	Rate (× 1 km^3 / Myr)	σ
Pliocene - Pleistocene	5.33 - 0	16 673.6	± 5 940.0	3 145.9	± 1 120.8
Aquitanian - Messinian	23.03 - 5.33	8 671.7	± 2 616.8	489.1	± 147.6
Rupelian - Chattian	33.9 - 23.03	8 938.4	± 2 301.7	822.3	± 211.7
Danian - Priabonian	66 - 33.9	17 198.3	± 5 915.2	535.8	± 184.3

883 **Table 1**

884 **Table 2 caption:** Percentage of carbonates for the studied time interval

Carbonate fraction for the Bay of Biscay

Time interval	(Ma)	Carbonate fraction (%)	σ
Pliocene - Pleistocene	5.33 - 0	7.5	± 7.5
Messinian	7.24 - 5.33	14	± 10
Aquitanian - Tortonian	23.03 - 7.24	18	± 10
Rupelian - Chattian	33.9 - 23.03	44	± 15
Danian - Priabonian	66 - 33.9	60	± 20

Carbonate fraction for the «Façade Atlantique» Basin

Time interval	(Ma)	Carbonate fraction (%)	σ
Pliocene - Pleistocene	5.33 - 0	5	± 5
Tortonian - Messinian	11.63 - 5.33	10	± 10
Langhian - Serravallian	15.97 - 11.63	20	± 20
Burdigalian	20.44 - 15.97	50	± 20
Aquitanian	23.03 - 20.44	60	± 30
Rupelian - Chattian	33.9 - 23.03	40	± 20
Priabonian	37.8 - 33.9	50	± 20
Danian - Bartonian	66 - 37.8	40	± 20

Carbonate fraction for the Arzacq Basin

Time interval	(Ma)	Carbonate fraction (%)	σ
Pliocene - Pleistocene	5.33 - 0	5	± 5
Tortonian - Messinian	11.63 - 5.33	10	± 10
Langhian - Serravallian	15.97 - 11.63	20	± 20
Burdigalian	20.44 - 15.97	50	± 20
Aquitanian	23.03 - 20.44	60	± 30
Rupelian - Chattian	33.9 - 23.03	20	± 10
Priabonian	37.8 - 33.9	20	± 10
Danian - Bartonian	66 - 37.8	40	± 20

Carbonate fraction for the Carcassonne Basin

Time interval	(Ma)	Carbonate fraction (%)	σ
Pliocene - Pleistocene	5.33 - 0	5	± 5
Tortonian - Messinian	11.63 - 5.33	10	± 10
Langhian - Serravallian	15.97 - 11.63	20	± 20
Burdigalian	20.44 - 15.97	50	± 20
Aquitanian	23.03 - 20.44	60	± 30
Rupelian - Chattian	33.9 - 23.03	25	± 20
Priabonian	37.8 - 33.9	20	± 20
Danian - Bartonian	66 - 37.8	40	± 20

Carbonate fraction for the Tarbes Basin

Time interval	(Ma)	Carbonate fraction (%)	σ
Pliocene - Pleistocene	5.33 - 0	5	± 5
Tortonian - Messinian	11.63 - 5.33	10	± 10
Langhian - Serravallian	15.97 - 11.63	20	± 20
Burdigalian	20.44 - 15.97	50	± 20
Aquitanian	23.03 - 20.44	60	± 30
Rupelian - Chattian	33.9 - 23.03	20	± 10
Priabonian	37.8 - 33.9	15	± 10
Danian - Bartonian	66 - 37.8	40	± 20

Carbonate fraction for the Aquitaine platform

Time interval	(Ma)	Carbonate fraction (%)	σ
Pliocene - Pleistocene	5.33 - 0	5	± 5
Tortonian - Messinian	11.63 - 5.33	10	± 10
Langhian - Serravallian	15.97 - 11.63	20	± 20
Burdigalian	20.44 - 15.97	50	± 20
Aquitanian	23.03 - 20.44	60	± 30
Rupelian - Chattian	33.9 - 23.03	20	± 10
Priabonian	37.8 - 33.9	15	± 10
Danian - Bartonian	66 - 37.8	40	± 20

Carbonate fraction for the Castres Basin

Time interval	(Ma)	Carbonate fraction (%)	σ
Pliocene - Pleistocene	5.33 - 0	5	± 5
Tortonian - Messinian	11.63 - 5.33	10	± 10
Langhian - Serravallian	15.97 - 11.63	20	± 20
Burdigalian	20.44 - 15.97	50	± 20
Aquitanian	23.03 - 20.44	60	± 30
Rupelian - Chattian	33.9 - 23.03	40	± 20
Priabonian	37.8 - 33.9	40	± 20
Danian - Bartonian	66 - 37.8	40	± 20

Carbonate fraction for the Tartas Mirande Basin

Time interval	(Ma)	Carbonate fraction (%)	σ
Pliocene - Pleistocene	5.33 - 0	5	± 5
Tortonian - Messinian	11.63 - 5.33	10	± 10
Langhian - Serravallian	15.97 - 11.63	20	± 20
Burdigalian	20.44 - 15.97	50	± 20
Aquitanian	23.03 - 20.44	60	± 30
Rupelian - Chattian	33.9 - 23.03	30	± 20
Priabonian	37.8 - 33.9	50	± 10
Danian - Bartonian	66 - 37.8	40	± 20

885 **Table 2**

886

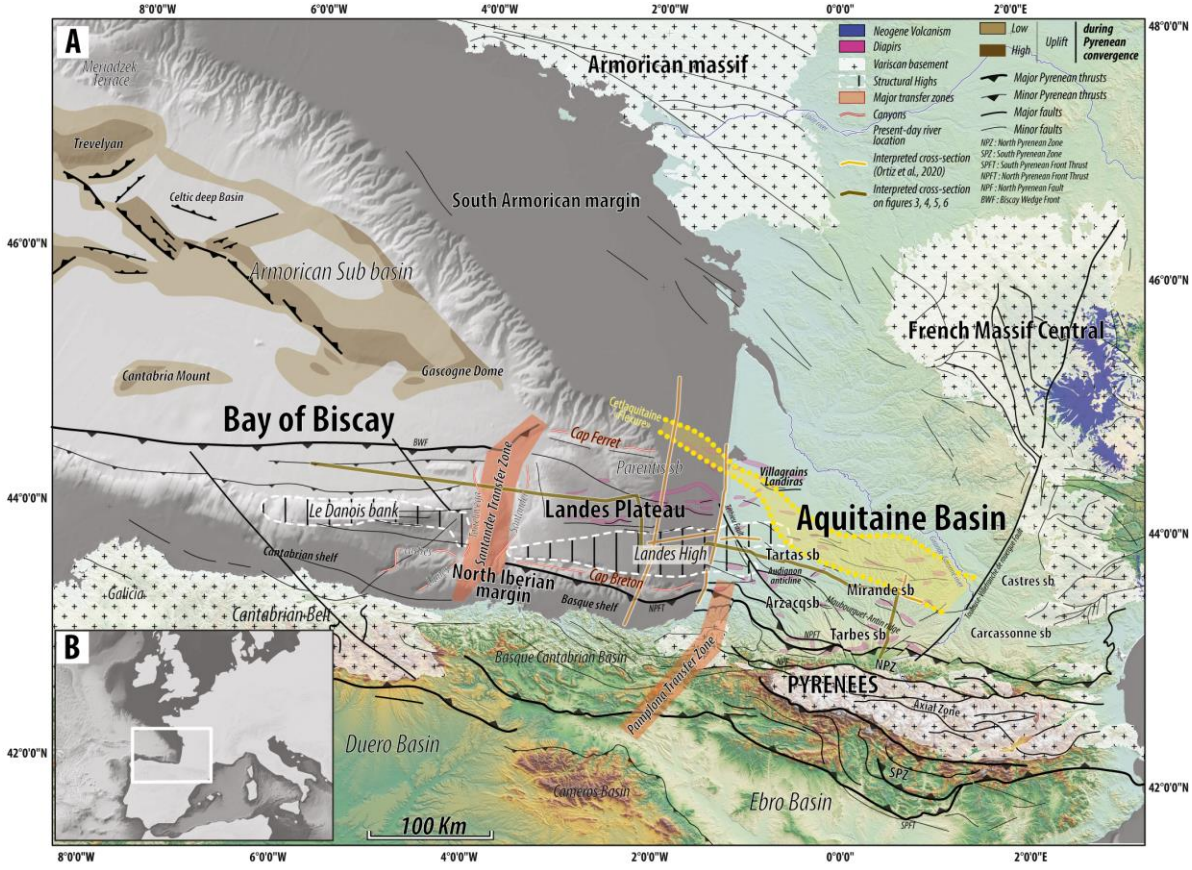
A
B
Armorican massif
South Armorican margin
Armorican Sub basin
Celtic deep Basin
Meriadzek Terrace
Trevelyan
Cantabria Mount
Gascogne Dome
Bay of Biscay
French Massif Central
Aquitaine Basin
Landes Plateau
Landes High
Le Danois bank
Cap Ferret
Parentis sb
Villagrains Landiras
Tartas sb
Mirande sb
Arzacqsb
Tarbes sb
Castres sb
Carcassonne sb
Cap Breton
North Iberian margin
Cantabrian shelf
Basque shelf
Galicia
Cantabrian Belt
Basque Cantabrian Basin
Pamplona Transfer Zone
PYRENEES
Duero Basin
Cameros Basin
Ebro Basin
100 Km
Neogene Volcanism
Diapirs
Variscan basement
Structural Highs
Major transfer zones
Canyons
Present-day river location
Interpreted cross-section (Ortiz et al., 2020)
Interpreted cross-section on figures 3, 4, 5, 6
Low
High
Uplift
during Pyrenean convergence
Major Pyrenean thrusts
Minor Pyrenean thrusts
Major faults
Minor faults
NPZ : North Pyrenean Zone
SPZ : South Pyrenean Zone
SPFT : South Pyrenean Front Thrust
NPFT : North Pyrenean Front Thrust
NPF : North Pyrenean Fault
BWF : Biscay Wedge Front
8°0'0"W
6°0'0"W
4°0'0"W
2°0'0"W
0°0'0"
2°0'0"E
48°0'0"N
46°0'0"N
44°0'0"N
42°0'0"N

887 **Figure 1**

888 **Figure 1:** A: Main physiographic and structural features and available dataset of seismic
889 reflection lines in the Aquitaine Basin, Landes Plateau and Biscay Bay deep-basin. B: Location
890 of the studied area in Europe.
891
892
893
894
895
896
897
898
899
900
901
902
903
904
905
906
907
908
909
910
911

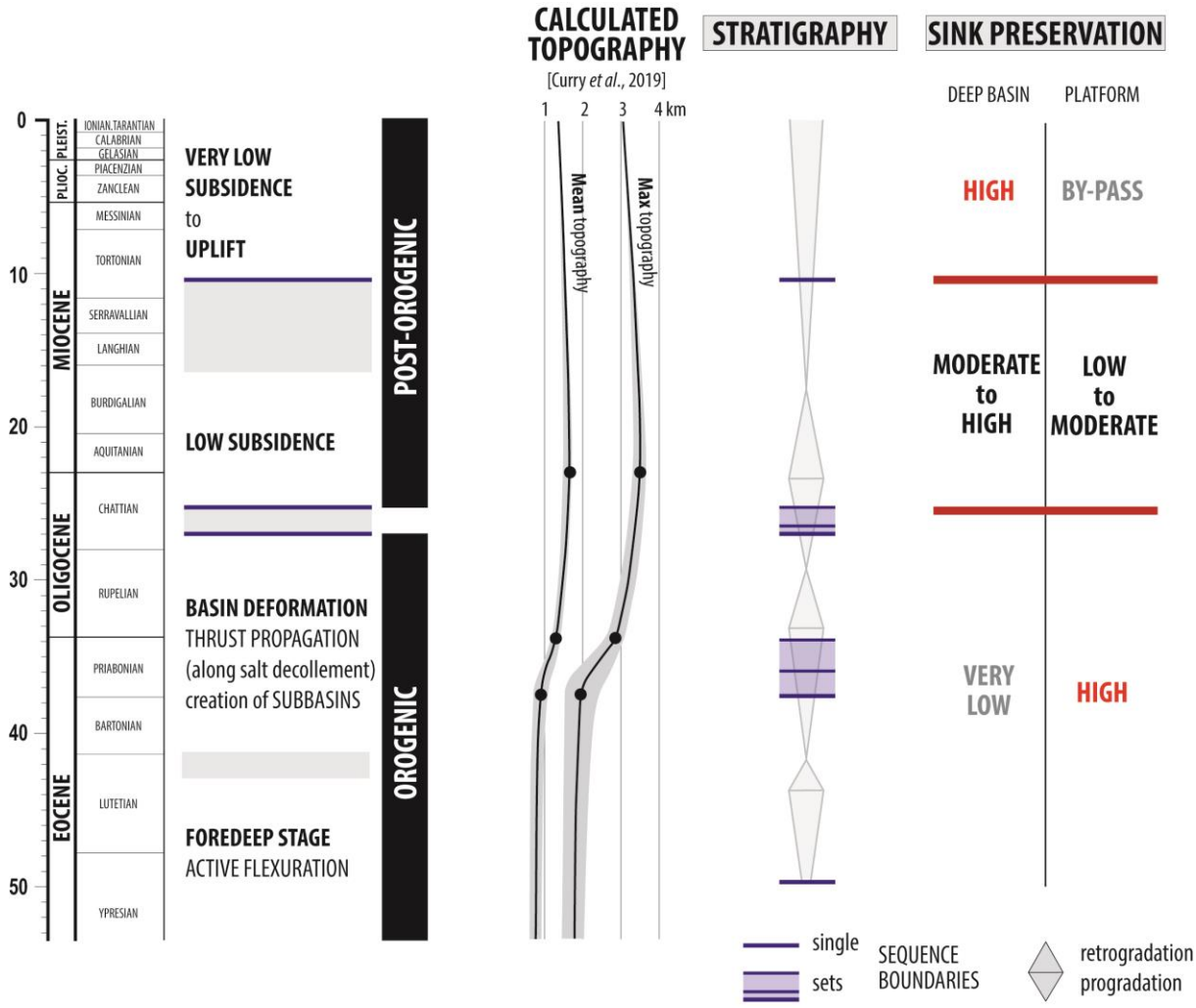

912 **Figure 2**

913

Figure 2: Synthetic chart of the main events (deformation, topography, sediment routing) of the Aquitaine Basin to deep Biscay Bay Basin sedimentary system

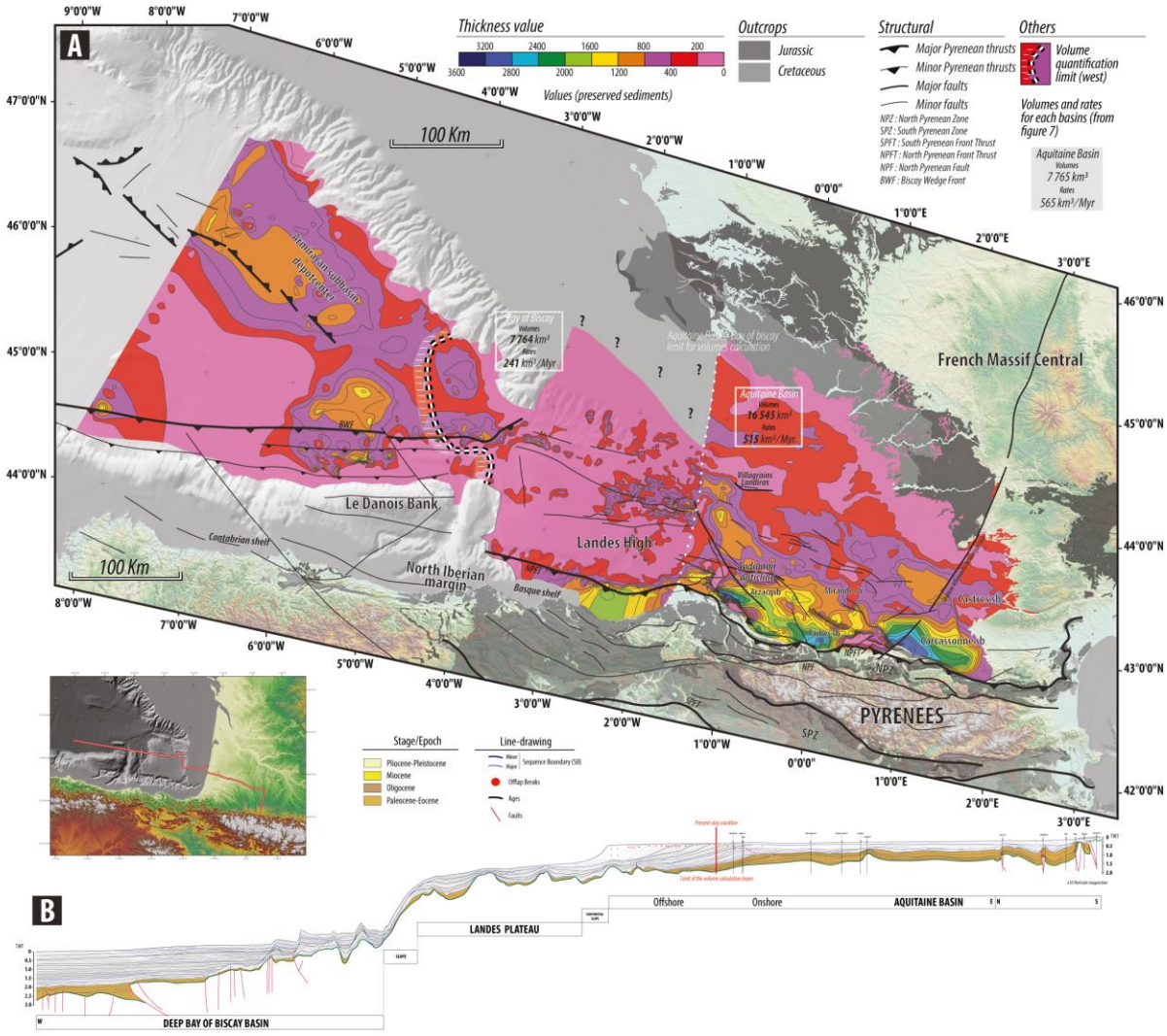
A
B
Thickness value
3200 2400 1600 800 200
3600 2800 2000 1200 400 0
Values (preserved sediments)
Outcrops
Jurassic
Cretaceous
Structural
Major Pyrenean thrusts
Minor Pyrenean thrusts
Major faults
Minor faults
NPZ : North Pyrenean Zone
SPZ : South Pyrenean Zone
SPFT : South Pyrenean Front Thrust
NPFT : North Pyrenean Front Thrust
NPF : North Pyrenean Fault
BWF : Biscay Wedge Front
Others
Volume quantification limit (west)
Volumes and rates for each basins (from figure 7)
Aquitaine Basin
Volumes
7 765 km³
Rates
565 km³/Myr
100 Km
Bay of Biscay
Volumes
7 764 km³
Rates
241 km³/Myr
Aquitaine Basin
Volumes
16 545 km³
Rates
575 km³/Myr
Le Danois Bank
Landes High
North Iberian margin
Cantabrian shelf
Basque shelf
French Massif Central
PYRENEES
Villagrains Landiras
Audignon outcrops
Arzacq sb
Mirandole
Castets sb
Carcassonne sb
Stage/Epoch
Pliocene-Pleistocene
Miocene
Oligocene
Paleocene-Eocene
Line-drawing
Sequence Boundary (SB)
Offlap Breaks
Ages
Faults
Offshore
Onshore
AQUITAINE BASIN
LANDES PLATEAU
DEEP BAY OF BISCAY BASIN

Figure 3

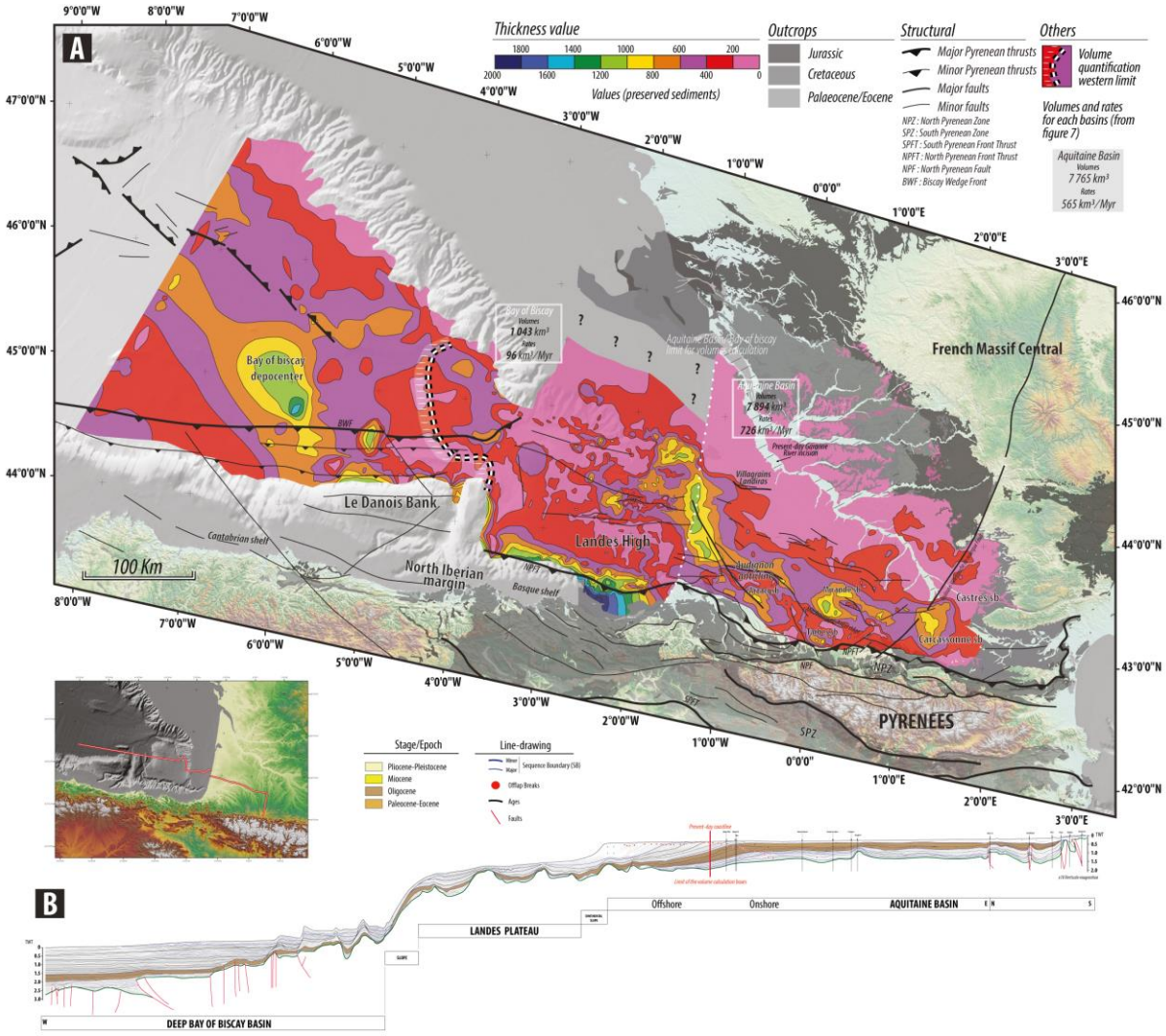
A
Thickness value
1800 1400 1000 600 200
2000 1600 1200 800 400 0
Values (preserved sediments)
Outcrops
Jurassic
Cretaceous
Palaeocene/Eocene
Structural
Major Pyrenean thrusts
Minor Pyrenean thrusts
Major faults
Minor faults
NPZ : North Pyrenean Zone
SPZ : South Pyrenean Zone
SPFT : South Pyrenean Front Thrust
NPFT : North Pyrenean Front Thrust
NPF : North Pyrenean Fault
BWF : Biscay Wedge Front
Others
Volume quantification western limit
Volumes and rates for each basins (from figure 7)
Aquitaine Basin
Volumes
7 765 km³
Rates
565 km³/Myr
Bay of biscay
Volumes
1 043 km³
Rates
96 km³/Myr
Aquitaine Basin - Bay of biscay
Volumes
7 894 km³
Rates
726 km³/Myr
Bay of biscay depocenter
BWF
Le Danois Bank
Cantabrian shelf
100 Km
North Iberian margin
Basque shelf
Landes High
French Massif Central
PYRENEES
NPF
NPZ
SPZ
Stage/Epoch
Pliocene-Pleistocene
Miocene
Oligocene
Paleocene-Eocene
Line-drawing
Sequence Boundary (SB)
Offlap Breaks
Ages
Faults
B
Offshore
Onshore
AQUITAINE BASIN
LANDES PLATEAU
DEEP BAY OF BISCAY BASIN

938 **Figure 4**

Figure 3: A: Palaeocene-Eocene preserved sediment thickness (isopach, meters) map. The volume quantification western limit is according to the deep sea fan location (Cremer, 1983; Iglesias, 2009). B: interpreted cross-section from the proximal Aquitaine Basin part to the deep Bay of Biscay Basin, the considered period (isopach map) is highlighted by colour in the cross-section.

Figure 4: A: Oligocene preserved sediment thickness (isopach, meters) map. The volume quantification western limit is according to the deep sea fan location (Cremer, 1983; Iglesias, 2009). B: interpreted cross-section from the proximal Aquitaine Basin part to the deep Bay of Biscay Basin, the considered period (isopach map) is highlighted by colour in the cross-section.

987

988

989

990

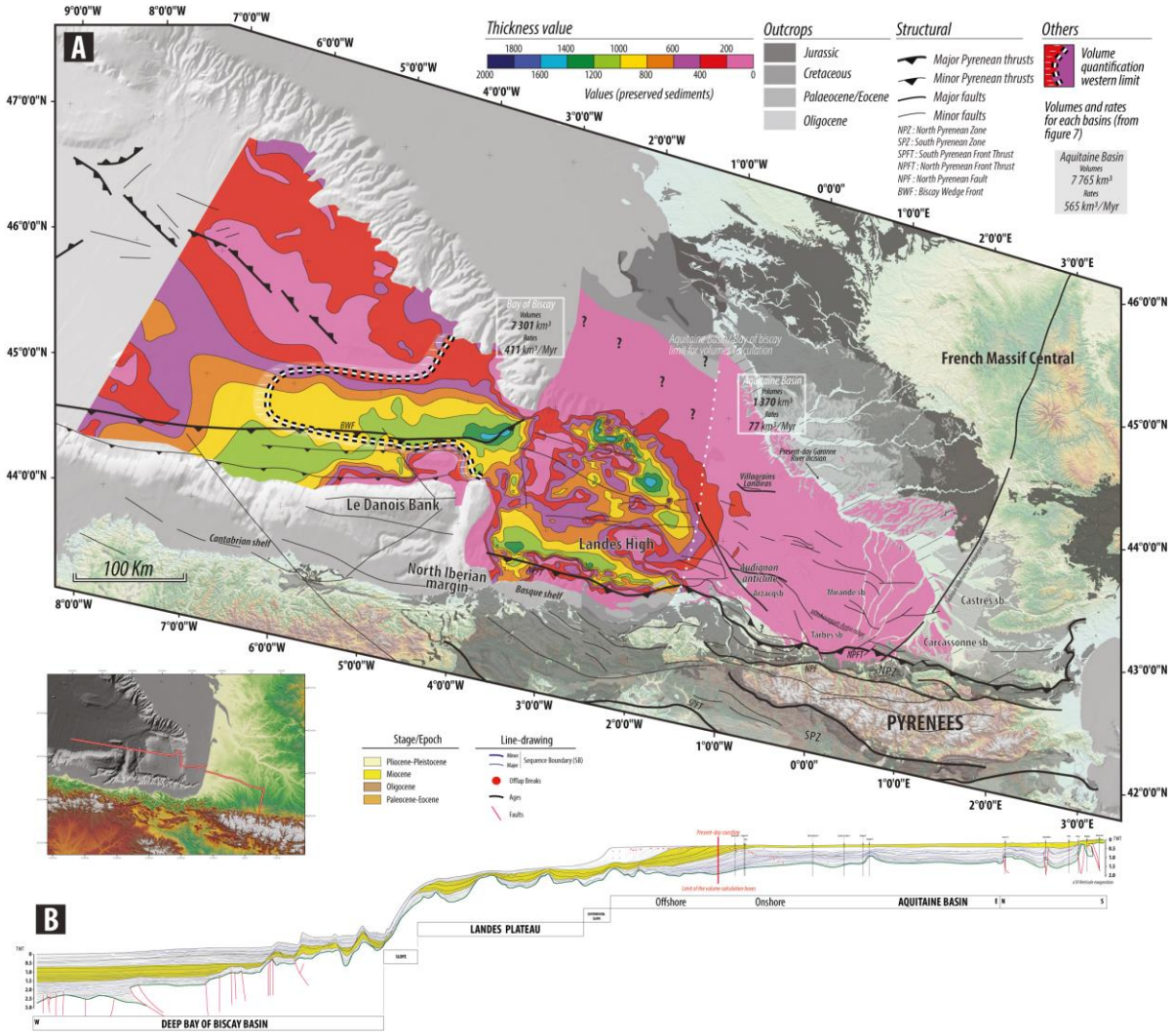
A
Thickness value
1800 1400 1000 600 200
2000 1600 1200 800 400 0
Values (preserved sediments)
Outcrops
Jurassic
Cretaceous
Palaeocene/Eocene
Oligocene
Structural
Major Pyrenean thrusts
Minor Pyrenean thrusts
Major faults
Minor faults
NPZ : North Pyrenean Zone
SPZ : South Pyrenean Zone
SPFT : South Pyrenean Front Thrust
NPFT : North Pyrenean Front Thrust
NPF : North Pyrenean Fault
BWF : Biscay Wedge Front
Others
Volume quantification western limit
Volumes and rates for each basins (from figure 7)
Aquitaine Basin
Volumes
7 765 km³
Rates
565 km³/Myr
Bay of Biscay
Volumes
7 301 km³
Rates
471 km³/Myr
Aquitaine Basin
Volumes
1 370 km³
Rates
77 km³/Myr
Aquitaine basin/Bay of biscay limit for volumes calculation
French Massif Central
Le Danois Bank
Landes High
North Iberian margin
Cantabrian shell
Basque shelf
BWF
NPF
SPFT
NPFT
SPZ
NPZ
PYRENEES
Villagrains Landiras
Present-day Garonne River incision
Audignon anticline
Mirande sb
Castres sb
Tarbes sb
Carcassonne sb
100 Km
Stage/Epoch
Pliocene-Pleistocene
Miocene
Oligocene
Paleocene-Eocene
Line-drawing
Sequence Boundary (SB)
Offlap Breaks
Ages
Faults
B
Present-day coastline
Limit of the volume calculation basins
Offshore
Onshore
AQUITAINE BASIN
LANDES PLATEAU
DEEP BAY OF BISCAY BASIN

991 **Figure 5**

Figure 5: A: Miocene preserved sediment thickness (isopach, meters) map. The volume quantification western limit is according to the deep sea fan location (Cremer, 1983; Iglesias, 2009). B: interpreted cross-section from the proximal Aquitaine Basin part to the deep Bay of Biscay Basin, the considered period (isopach map) is highlighted by colour in the cross-section.

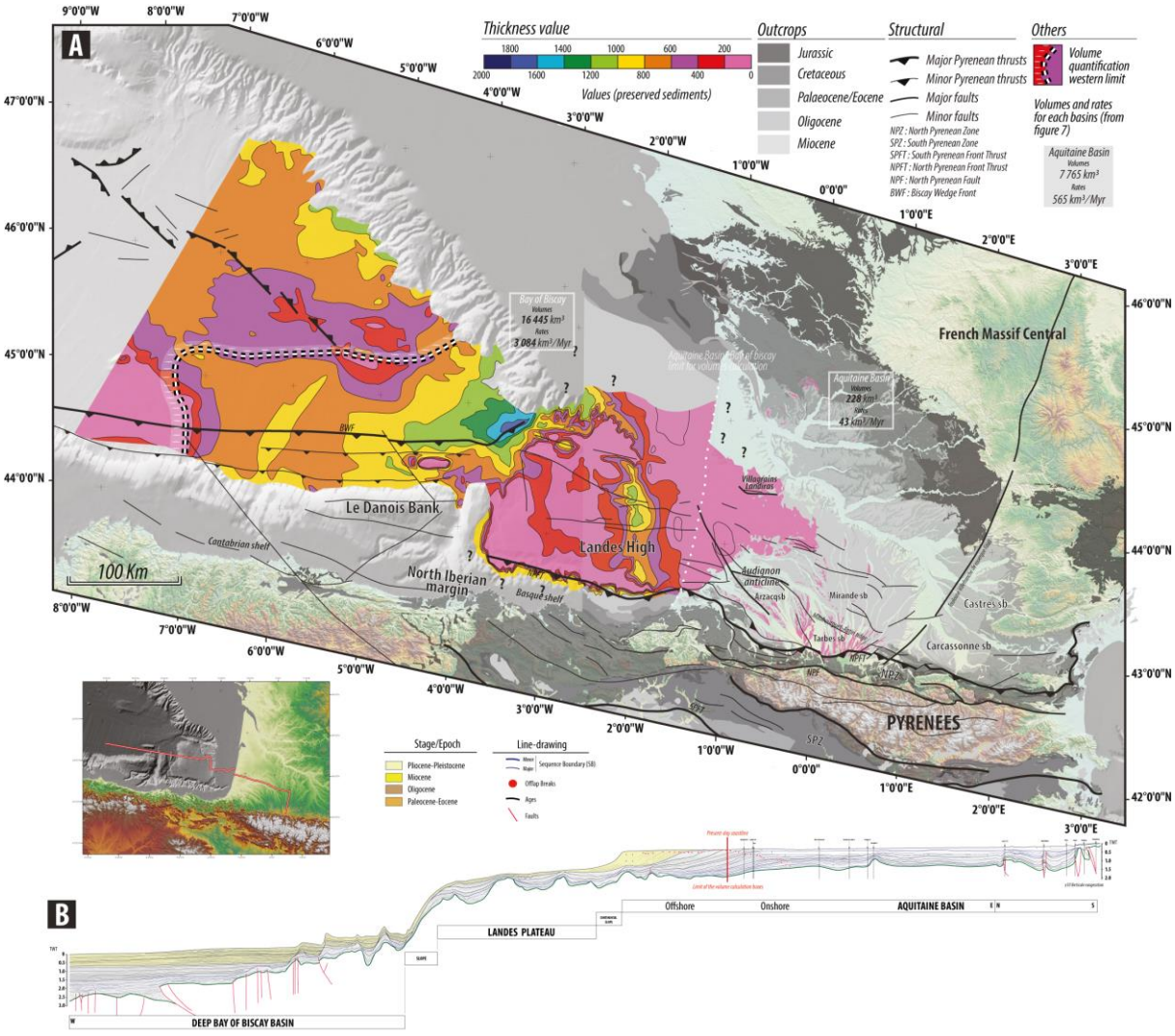
A
Thickness value
1800 1400 1000 600 200
2000 1600 1200 800 400 0
Values (preserved sediments)
Outcrops
Jurassic
Cretaceous
Palaeocene/Eocene
Oligocene
Miocene
Structural
Major Pyrenean thrusts
Minor Pyrenean thrusts
Major faults
Minor faults
NPZ : North Pyrenean Zone
SPZ : South Pyrenean Zone
SPFT : South Pyrenean Front Thrust
NPFT : North Pyrenean Front Thrust
NPF : North Pyrenean Fault
BWF : Biscay Wedge Front
Others
Volume quantification western limit
Volumes and rates for each basins (from figure 7)
Aquitaine Basin
Volumes
7 765 km³
Rates
565 km³/Myr
Bay of Biscay
Volumes
16 445 km³
Rates
3 084 km³/Myr
Aquitaine Basin
Volumes
228 km³
Rates
43 km³/Myr
French Massif Central
Le Danois Bank
Landes High
North Iberian margin
Cantabrian shell
Basque shell
BWF
NPF
SPZ
NPFT
Villagrains Landiras
Audignon anticline
Arzacqsb
Mirande sb
Castres sb
Tarbes sb
Carcassonne sb
PYRENEES
100 Km
Stage/Epoch
Pliocene-Pleistocene
Miocene
Oligocene
Paleocene-Eocene
Line-drawing
Sequence Boundary (SB)
Offlap Breaks
Ages
Faults
B
Offshore
Onshore
AQUITAINE BASIN
LANDES PLATEAU
DEEP BAY OF BISCAY BASIN

Figure 6

Figure 6: A: Pliocene-Pleistocene preserved sediment thickness (isopach, meters) map. The volume quantification western limit is according to the deep sea fan location (Cremer, 1983; Iglesias, 2009, Brocheray et al., 2014). B: interpreted cross-section from the proximal Aquitaine Basin part to the deep Bay of Biscay Basin, the considered period (isopach map) is highlighted by colour in the cross-section.

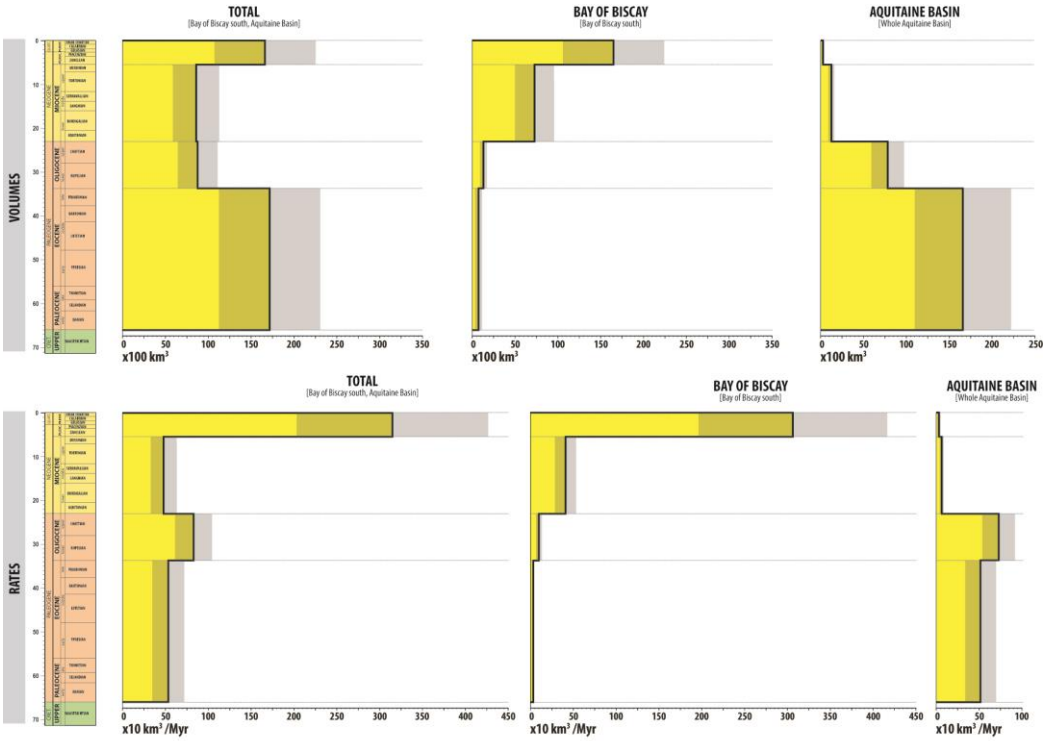
VOLUMES
TOTAL
[Bay of Biscay south, Aquitaine Basin]
BAY OF BISCAY
[Bay of Biscay south]
AQUITAINE BASIN
[Whole Aquitaine Basin]
x100 km³
RATES
TOTAL
[Bay of Biscay south, Aquitaine Basin]
BAY OF BISCAY
[Bay of Biscay south]
AQUITAINE BASIN
[Whole Aquitaine Basin]
x10 km²/Myr

Figure 7

Figure 7: Siliciclastic sedimentation volumes and rates of the Aquitaine Basin and Bay of Biscay.

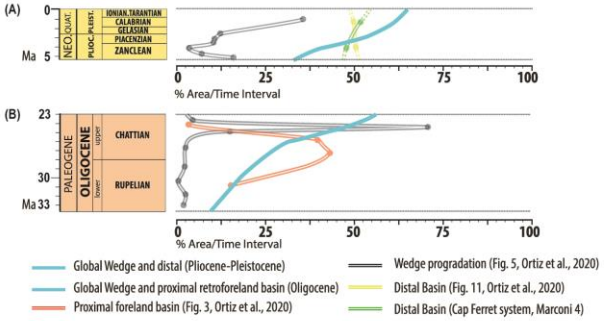

Figu re 8

1073

1074

Figure 8: In the cross sections published in Ortiz et al., (2020), some parts of the interpretation are of higher resolution than the resolution of the calculations in this paper (i.e. Palaeocene-Eocene, Oligocene, Miocene, Pliocene-Pleistocene). For example, the figure 5 in Ortiz et al., (2020) shows several high resolutions surfaces (thanks to orbitostratigraphy) at 32.2, 32.0, 31.3, 29.4, 27.1, 26.4, 25.2, 24.5, 24.4 Ma for the Oligocene period. This resolution on different parts of the cross section allows us to make a precise quantification shown in the figure. This figure is a compilation of the percentage of 2D area normalized to their duration thanks to high resolution timeline on different cross section published in Ortiz et al., (2020)